International Journal of Mechanical Sciences 136 (2018) 321–338

Contents lists available at ScienceDirect

International Journal of Mechanical Sciences

journal homepage: www.elsevier.com/locate/ijmecsci

Hunting patterns and bifurcation characteristics of a three-axle locomotive bogie system in the presence of the flange contact nonlinearity

G.W. Luo [a,*], Y.Q. Shi [b], X.F. Zhu [b], S.S. Du [b]

[a] School of Mechanical and Electronical Engineering, Lanzhou University of Technology, Lanzhou 730050, PR China
[b] Key Laboratory of System Dynamics and Reliability of Rail Transport Equipment of Gansu Province, Lanzhou, 730070, PR China

ARTICLE INFO

Keywords:
Three-axle locomotive bogie
Vibro-impact
Hunting motion
Bifurcation
Occurrence region

ABSTRACT

This paper considers a three-axle railway locomotive bogie running on a straight track and presents pattern diversity and bifurcation characteristics of its hunting behaviors at forward speeds higher than the hunting critical speed. Poincaré sections describing the cycle characteristic and wheel-rail impacts of the bogie system are defined according to the geometric structure of phase space of the dynamical system for carrying out multi-target and multi-parameter co-simulation analysis. The influences of dynamical parameters of the locomotive bogie on the wheel–rail impacts are studied and some important features of hunting behaviors in the presence of the flange contact nonlinearity are found. A series of grazing bifurcations induce the pattern diversity of hunting behaviors. The impacts of the middle and trailing wheelsets on the rail fall behind that of the leading wheelset, and the impact lag of the hunting motion of the middle wheelset is the most obvious of the three wheelsets. The top branch of impact velocity bifurcation diagram of period 1 hunting motion of the trailing wheelset is slightly lower than those of the leading and middle wheelsets. The instability speed of period 1 hunting-impact motion of the bogie system with worn wheelsets is lower than that with new wheelsets and the impact velocities of the worn wheelsets on the rail become smaller. A method of reasonable matching of primary suspension parameters, which brings about the substantial increase of the instability speed of periodic hunting behavior in the presence of the flange forces, is presented and the matching effect is verified by bifurcation diagrams of impact velocities of the new and worn leading wheelsets versus the forward speed.

1. Introduction

With the increase of the forward speeds of railway vehicles, vehicle designers are interested in achieving higher critical hunting speeds of the vehicles they design than before. High-speed trains need to have a higher critical speed. If the train loses its stability, the hunting motion will appear in the operation. The severe hunting motion will deteriorate the running quality of the railway vehicles, reduce ride comfort, lead to strong interactions between wheels and rails, and even cause derailment in a major accident. In everyday operation, the locomotive and cars usually do not run at speeds which are higher than the critical speed. It may, however, happen that the critical speed has decreased below the operating speed due to heavily worn wheel profiles or other reasons, so there is a demand to further know what can happen for the railway vehicles running at speeds which are higher than the corresponding critical speeds. Some studies can be found on railway vehicle lateral stability, hunting bifurcation behaviors and chaotic hunting motions. Cooperrider [1] first formulated the railway vehicle systems and reported the results of an analysis of nonlinear equations of motion written for a railway truck, including the influence of the nonlinear effects on stability, the character of the hunting motion, the effects of flange contact, wheel slip and Coulomb friction described by nonlinear expressions, etc. Nó and Hedrick [2] discussed the problem of maximizing the critical speed through design of the primary and secondary suspension but with control only over the range of wheel/rail geometry and friction characteristics. Kaas-Petersen et al. [3,4] studied the hunting motion in the complex Cooperrider bogie, both with and without the flange force that was represented as a very stiff spring with a dead band. They found symmetry-breaking bifurcations in the model without the flange force and chaotic motions in the latter model with flanged wheels. True et al. [5,6] put forward an improved dynamical model on the basis of the Cooperrider bogie, analyzed the asymmetry-breaking bifurcation, Neimark–Sack bifurcation, saddle-node bifurcation and pitchfork bifurcation appearing in the symmetric railway bogie system and discussed the mode interactions near a degenerate bifurcation. On the basis of the parameter study of hunting and chaos in railway vehicle dynamics [7], True [8] defined various equilibrium states of railway vehicle systems, discussed the important case of multiple equilibrium states and their dependence on parameters, and presented the applications in vehicle simulations. Zeng [9] put forward a numerical computation method for

* Corresponding author.
E-mail addresses: luogw@mail.lzjtu.cn, luogw@lut.cn (G.W. Luo).

https://doi.org/10.1016/j.ijmecsci.2017.12.022
Received 17 August 2017; Received in revised form 3 December 2017; Accepted 11 December 2017
Available online 19 December 2017
0020-7403/

Hopf bifurcation and limit cycles of railway vehicle systems through using the QR algorithm to calculate the eigenvalues of the first approximate system incorporating with the Gold Cut method. Ahmadian and Yang [10] investigated the effect of system parameters on hunting of a rail vehicle with nonlinear yaw dampers and wheel–rail interface and found that the flange contact nonlinearities brought about a significant effect on the hunting behavior. In Ref. [11], they also presented an analytical investigation of Hopf bifurcation and hunting behavior of a rail wheelset with nonlinear primary yaw dampers and wheel–rail contact forces and investigated the nonlinearities stemming from creep–creep force saturation and nonlinear contacts between a realistic wheel and rail profile. Yang and Shen demonstrated the stability and Hopf bifurcation of hunting motion of a locomotive bogie with hysteretic and nonlinear suspensions in their monograph [12]. Using the method of multiple scales, Kim and Seok [13] unfolded a bifurcation analysis on a nonlinear railway vehicle having dual-bogies to examine the coupling effect of the bogies on the vehicle's hunting behavior. Based on hunting stability analysis of high-speed railway vehicle trucks on curved tracks [14], Lee and Cheng derived the nonlinear coupled differential equations of the motion of the truck systems with different degrees of freedom and moving on curved tracks, compared the influences of the suspension parameters on the critical hunting speeds evaluated via the linear and nonlinear creep models [15], and analyzed the respective effects of the major system parameters on the vehicle dynamics [16], and presented the desired regions of suspension parameters in which critical hunting speeds exceed 300 km/h obtained using the 14-DOF and 24 DOF models [17]. Zboinski and Dusza [18] presented a new method suitable for analysis on nonlinear lateral stability of rail vehicles in a curved track. They extended the study of the stability as compared with the method used by the them and discussed differences between results obtained with the earlier and extended approaches [19], and further presented the extended use of the method worked out by them to bifurcation analysis of more complex rail vehicle models [20]. Hoffmann [21] analyzed dynamics of European two-axle freight wagons with the UIC standard suspension through the use of a multibody model developed specifically for revealing the complex hunting behavior in the running properties of freight wagons. The dynamical investigations of the European two-axle railway wagons were extended to the behaviour in curves by Gialleonardo et al. [22]. Zhai and Wang [23] considered the viscoelastic property of railway track structure and investigated the effect of track system properties such as the rail fastener stiffness and the rail profile on the lateral hunting stability of a freight car with three-piece bogies. They found out the differences of the critical hunting speeds of vehicles on rigid track model and on elastic track model and carried out a full-scale field experiment to investigate the hunting behavior of the freight car on a straight track. Based on wheel/rail coupled dynamics [23], Wang and Liu [24] developed a model to simulate dynamic performance of the heavy-haul vehicle on curved track, and put forward a bifurcation diagram for the vehicle with three-piece bogies on the curved track to determine the nonlinear critical speed and the hunting motion of the heavy-haul vehicle appearing due to the larger conicity, the initial lateral shift and the wheelset angle of attack. Gao and Li et al. [25] investigated the lateral bifurcation behavior of a high-speed four-axle railway passenger in large speed ranges and obtained its stable and unstable orbits and linear and nonlinear critical speeds. Subsequently, the two-axle bogie system with the flange forces is taken as the analysis object in Refs. [26,27], several kinds of nonlinear dynamical phenomena, such as stationary equilibrium point, symmetric or asymmetric periodic oscillations, and symmetric or asymmetric chaotic motions, are found and discussed in great detail from the point of the mathematics or mechanics. Recently, True [28] discussed the easier numerical methods proposed to find the critical speed in railway dynamical problems, and put forward the algorithm on finding multiple attractors and critical parameters. Choi and Shin [29] considered the flange contact when lateral displacement exceeds the dead band between wheel flange and rail and devised direct numerical integration and a shooting algorithm to calculate the response of a high-speed train. They found that the critical speed increases as the creep curve becomes stiff before saturation, which is more effective than the variation in suspension parameters. At present, the wheel–rail impact dynamics mainly focuses on the studies considering the contribution due to the pitch and roll motions of the car body and bogies. Effects of primary and secondary suspension's stiffness on wheel–rail impact force have been investigated by Nielsen and Igeland [30], Dong [31], Sun and Dhanasekar [32]. These studies concluded that vehicle suspension properties do not have significant effects on wheel–rail impact loads. This assumption has been confirmed by both analytical and experimental data as shown in [31]. Uzzal et al. [33] investigated dynamic contact loads at wheel–rail contact point in a three-dimensional railway vehicle–track model as well as dynamic response at vehicle–track component levels in the presence of wheel flats. They considered the idealized Haversine wheel flats with the rounded corner in the wheel–rail contact model and investigated the wheel–rail impact forces arising in the wheel–rail interface due to the presence of wheel flats. The wheel–rail impact properties that arise in the wheel–rail interface due to the presence of the flange contact nonlinearities are included in a very few studies [34,35]. Definitely, the primary suspension parameters and wheel and rail profile parameters have effect on lateral dynamic behavior of the vehicle running on the rails, including the vehicle lateral hunting stability, hunting pattern diversity and bifurcation characteristics, as seen in more relevant researches [36–42]. It is necessary to further understand, however, how strong the effect these parameters on the hunting motions with the flange forces is, and which parameters have a significant influence on such hunting motions.

This study is primarily concerned with diversity and bifurcation characteristics of hunting motions of a three-axle railway locomotive bogie considering the contribution due to the yaw and lateral motions of the frame and wheelsets in the presence of the flange contact nonlinearities. The remainder of this paper is organized as follows. Section 2 introduces the nonlinear wheel–rail contact geometry relation, the normal contact forces between the wheelset and the rail, dynamical model and its corresponding differential equations of hunting behaviors of the locomotive bogie system. In Section 3, a numerical analysis based on the Poincaré sections describing the characteristics of lateral dynamic behaviors of the bogie system running on the rails is proposed to ascertain the basic patterns, characteristics and diversity of hunting behaviors of the leading, middle and trailing wheelsets and the frame. In Section 4, the incidence relation between hunting patterns and bifurcation characteristics of the bogie system and its key dynamical parameters is studied by multi-objective and multi-parameter co-simulation analysis, the influence of the primary suspension stiffness and the equivalent conicity of wheel tread on the impact of the wheelsets on the rail is discussed, and the stiffness matching of the primary suspension, which brings about the increase of instability speed of period 1 hunting motion, is presented. Last section summarizes and concludes this paper.

2. Dynamical model of hunting behavior of the railway locomotive bogie

2.1. Wheel–rail contact geometry relation

Let us consider dynamical model of hunting behavior of a railway locomotive bogie, which is schematically represented in Fig. 1 [43,44]. The locomotive bogie system consists of a bogie frame, three wheelsets, the primary suspensions and the secondary suspension. The wheel–rail contact geometry relation, wheel–rail creep forces and flange forces between the wheelset and the rail are very important for the research on vehicle system dynamics and control. The geometry and contact relations between the wheelset and the rail need to be emphasized first. The cross-section parameters of the wheelset and rail can be introduced by a sketch map of a single wheelset reported in Fig. 2. The wheel–rail contact geometry parameters, which mainly include the rolling radius and the contact angle for the left and the right wheels, and the roll angle

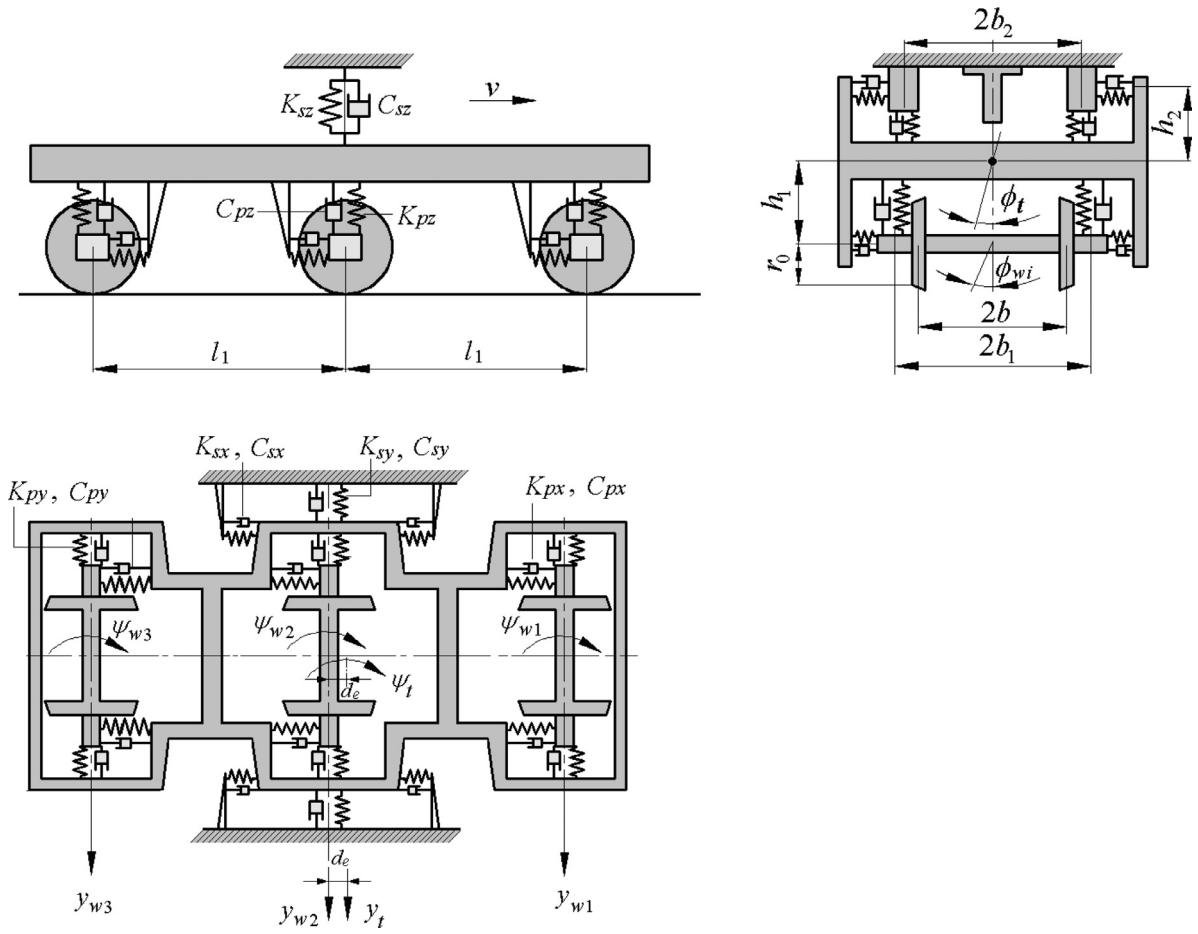

Fig. 1. Schematic representation of the model of a locomotive bogie for the study of the hunting motion.

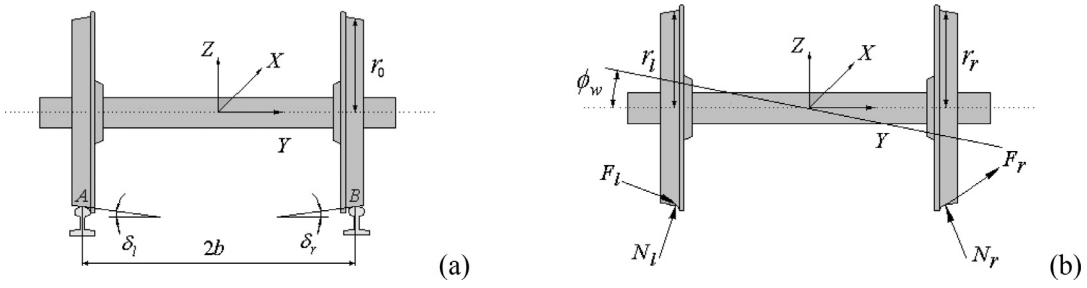

Fig. 2. The sketch map of a single wheel wheelset.

of the wheelset, can be approximately described by linear functions of the lateral displacement of the wheelset. In Fig. 2, r_0 is the nominal contact rolling radius of the wheel, r_l and r_r are the practical rolling radius of two wheels of the wheelset, and the subscripts l and r denote the left and right wheels of the wheelset, respectively; δ_0 is the contact angle related to the wheelset center situated at the vertical plane through the track centerline, δ_l and δ_r are the actual contact angle of the wheels. As a vehicle runs along the rail, the wheel–rail contact geometry relation, associated with the lateral deviation y_w of the wheelset, can be written by the following expressions

$$r_l,\ \ r_r = r_0 \pm \lambda\, y_w,\ \delta_l,\ \ \delta_r = \delta_0 \pm \varepsilon_0\, y_w/b,\ \phi_w = \sigma\, y_w/b, \tag{1}$$

where λ denotes the equivalent conicity of the wheel tread which gradually increases with the wear of the wheel, ε_0 represents a variable parameter of the contact angle due to the lateral displacement of the wheelset, σ is the parameter of the roll angle, ϕ_w denotes the roll angle of the wheelset, and b is half of the distance between the left and right contact points A and B of the wheelset and the rail. As for the same kind of rolling stocks, the geometry parameters above-mentioned are constant values.

In the contact forces between the wheelset and rail labeled in Fig. 2(b), $F_l(F_r)$ and $N_l(N_r)$ denote the tangential and normal contact forces corresponding to the contact point A (B) of the left (right) wheel' tread, respectively. These forces will be expounded in the ensuing section of this chapter.

2.2. The normal contact relation

There is an extremely complex physical phenomenon when the stiff wheels with elasticity move forward on the stiff rails with elasticity at a certain speed. The stiff wheels slide relatively to the stiff rails and therefore there are some velocity differences in the contact area between the wheels and the rails. The slip includes elastic deformation and rigid slip. It should be understood as micro-slip and indicates the local relative ve-

locity in the given point of the contact area between two rolling bodies. Generally, the relative sliding velocity is called the creep. The relative velocity or relative angular velocity in wheel–rail contact point normalized by the forward speed is denoted as the creepage, and the creep forces and creep torques are produced by the relative slip of wheel and rail on the contact area and rely heavily on the creepage. The longitudinal creepage ξ_x, the lateral creepage ξ_y and the spin creepage ξ_{sp} of the wheelset are written as follows [45]

$$\begin{aligned}\xi_{x(l,\,r)} &= \frac{v+\psi_w\dot{y}_w+r_{(l,\,r)}\left(\psi_w\dot{\phi}_w-\Omega\right)\mp b\dot{\psi}_w}{v},\\ \xi_{y(l,\,r)} &= \frac{-v\psi_w+\dot{y}_w+r_{(l,\,r)}\dot{\phi}_w}{v\cos\left(\delta_{(l,\,r)}\right)}\\ \xi_{sp(l,\,r)} &= \frac{\mp\left(\Omega-\psi_w\dot{\phi}_w\right)\sin\left(\delta_{(l,\,r)}\right)+\dot{\psi}_w\cos\left(\delta_{(l,\,r)}\right)}{v}.\end{aligned} \tag{2}$$

in which v is the forward running speed of the locomotive, ϕ_w is the roll angle of the wheelset, ψ_w denotes yaw angle of the wheelset, and Ω is called the nominal angular velocity of the wheel and $\Omega = v/r_0$; the subscript (l, r) denotes the left wheel and the right wheel of the wheelset, respectively; the upper and the lower in the signs $\pm$ and $\mp$ respectively correspond to the left wheel and the right wheel, and the description of the subscript (l, r) and the signs $\pm$ and $\mp$ are of the same meanings in the following expressions.

The Kalker's linear creep theory is put forward on the basis of small creep and small spin condition, i.e., the adhesive region dominates on the wheel–rail contact surface. According to the Kalker linear creep theory [46], the longitudinal creep force F_x, lateral creep force F_y and spin creep torque M_z in the contact patch of the wheel and rail, associated with the linear region, can be expressed as

$$F_x = -f_{11}\xi_x,\ F_y = -f_{22}\xi_y - f_{23}\xi_{sp},\ M_z = f_{23}\xi_y - f_{33}\xi_{sp}. \tag{3}$$

where the symbols f_{11}, f_{22}, f_{23} and f_{33} denote the longitudinal, lateral, lateral/spin, spin creep coefficients, respectively. The creep coefficients can be calculated easily, which are associated with the wheel–rail contact geometry parameters found in Kalker's contact table [47], i.e., the resultant shear modulus of the wheel and rail materials, the lengths of the major and minor semi-axes of the contact ellipse, and the Kalker coefficients.

The linear creep force components and the spin creep torque in the contact area are obtained from Eq. (3) when the creepages are calculated from Eq. (2). As for large creep condition at which the sliding region dominates on the wheel–rail contact surface, or even completely sliding case, the linear creepage/creep force relation between the wheel and rail will be inevitably broken. Consequently, the creep force cannot increase linearly with successive increase in the creepage, and the creepage/creep force relation exhibits nonlinearity until it finally trends toward the saturation limit represented by Coulomb's friction force. Therefore, the nonlinear creep theory put forward by Shen et al. [48] is applied in order to expand the linear results so that the nonlinear creep force can be calculated and the availability can also be extended to arbitrary value of the creepage, i.e., from zero up to total wheel slip. The revision coefficient ε is defined as

$$\varepsilon = \begin{cases}\left(\beta-\beta^2/3+\beta^3/27\right)/\beta & \beta\le 3\\ 1/\beta & \beta>3\end{cases}, \tag{4}$$

Here β is the normalized resultant creep force and can be calculated by

$$\beta = F/(\mu N) = \sqrt{F_x^2+F_y^2}/(\mu N), \tag{5}$$

where F is the resultant force of longitudinal creep force F_x and lateral creep force F_y, μ denotes the friction coefficient between the wheel and rail and N is the normal force in the contact area.

Then the revised creep forces and creep torques given in Refs. [43,48] are

$$F_x' = \varepsilon F_x,\ F_y' = \varepsilon F_y,\ M_x' = \varepsilon M_x. \tag{6}$$

It needs to be emphasized that the subscript symbols l and r denoting the left and right wheels have been omitted in Eqs. (3)–(6) for convenience and simplification in the description, because these equations are of universality for the wheel–rail systems. It is important to note that the revised creep forces and creep torques are obtained in the contact patch. However, the differential equations of lateral hunting motion of railway vehicle are generally established in the track coordinate system. The coordinate transformation between the contact coordinate system and the track coordinate system is provided to switch the revised creep forces and creep torques in the contact patch to the track coordinates [43,49]. The coordinate transformation can be achieved by the concrete expression

$$\begin{Bmatrix}F_{(l,\,r)x}\\ F_{(l,\,r)y}\\ M_{(l,\,r)z}\end{Bmatrix} = \begin{bmatrix}\cos(\psi_w) & -\cos(\delta_{(l,\,r)}\pm\phi_w)\sin(\psi_w) & 0\\ \sin(\psi_w) & \cos(\delta_{(l,\,r)}\pm\phi_w)\cos(\psi_w) & 0\\ 0 & 0 & \cos(\delta_{(l,\,r)}\pm\phi_w)\end{bmatrix}\begin{Bmatrix}F'_{(l,\,r)x}\\ F'_{(l,r)y}\\ M'_{(l,\,r)z}\end{Bmatrix}. \tag{7}$$

The force $N_{(l,\,r)}$ in the contact patch represents the normal contact force for the left (or right) wheel and the rail. On the straight track, the vertical components $N_{(l,\,r)z}$ of the normal contact forces are supposed to be the half of the axle load. Consequently, the lateral components can be computed by

$$N_{(l,\,r)y} = \mp N_{(l,\,r)}\sin(\delta_{(l,\,r)}\pm\phi_w),\ N_{(l,\,r)z} = N_{(l,\,r)}\cos(\delta_{(l,\,r)}\pm\phi_w), \tag{8}$$

where $N_{(l,\,r)z} = 0.5W$, W is the axle load.

There exists a lateral clearance η between the wheel flange and the rail, which is called the flange clearance. The lateral deviation y_w of the wheelset is restricted by the flange clearance during the hunting motion. As the lateral deviation of the wheelset gradually increases and exceeds the flange clearance, a lateral contact between the wheel flange and the rail inevitably occurs, which results in non-smooth changes in the dynamical properties. Consequently, the restoring force $F_t(y_w)$ is created along with the no-smooth contact between the wheel flange and the rail, which is called the flange force and can be approximately modeled by a piecewise linear function [3]

$$F_t(y_w) = \begin{cases}k_r(y_w-\eta) & y_w>\eta\\ 0 & |y_w|\le\eta\\ k_r(y_w+\eta) & y_w<-\eta\end{cases} \tag{9}$$

where y_w denotes the lateral displacement of the wheelset, K_r represents the flange contact stiffness and the original value presented by Cooperrider [1], $K_r = 146.0$ MN/m, is directly adopted in this paper.

The flange contact considered using the piecewise-linear function with a dead zone is a simplifying hypothesis. The wheel–rail contact geometry parameters expressed by Eq. (1) are linear functions of the lateral displacement of the wheelset, while other factors in wheel–rail contact, including λ, ε_0 and σ, are considered as constant and not dependent on the lateral position of the wheelset. In this paper, lateral dynamics of the locomotive bogie is studied with emphasis on pattern diversity and transition characteristics of its hunting behaviors from the new wheelset to the worn wheelset, i.e., the influence of wheel–rail wear on hunting behaviors in the presence of the flange forces. In this way, the equivalent conicity of the wheel tread is one of the key parameters, so we adopt the approximate model of flange force (9) and the linear wheel–rail contact geometry parameters (1) for facilitating multi-object and multi-parameter collaborative simulation. As for the influence of suspension parameters on hunting behaviors, the nonlinear wheel–rail contact geometry parameters, depending on lateral displacement of the wheelset, may also be considered for the more accurate descriptions of the wheel–rail contact properties, which can be actualized by adopting

the wheel–rail contact table from RSGEO [50] for the determination of the kinematic contact values.

2.3. Dynamical model

A three-axle railway locomotive bogie is considered and its dynamics is studied with emphasis on bifurcation behaviors of the hunting motion. Dynamical model of hunting behavior of the locomotive bogie system is schematically shown in Fig. 1. The suspension elements in the model are assumed to be of the linear elastic characteristics. As shown in Fig. 1, the bogie frame is supported on three wheelsets by the primary suspensions consisting of the linear springs with stiffness K_{px}, K_{py} and K_{pz} and linear viscous dashpots with damping constant C_{px}, C_{py} and C_{pz}. Similarly, the secondary suspension elements between the bogie frame and the car body are composed of the linear springs with stiffness K_{sx}, K_{sy} and K_{sz} and linear viscous dashpots with damping constant C_{sx}, C_{sy} and C_{sz}. The car body is supposed to move along the track centerline with the forward speed v. As for the analysis of lateral hunting stability and bifurcation of the railway locomotive bogie, all the parts except the primary and secondary suspension elements can be assumed to be rigid bodies. As we known from Eq. (9), when the lateral deviation of the wheelset gradually increases and exceeds the flange clearance, a contact between the wheel flange and the rail occurs, which results in non-smooth changes in the dynamical properties of the bogie system. Consequently, dynamical model illustrated in Fig. 1 is a nine-degree-of-freedom nonlinear system with non-smooth characteristics resulted from the impacts between the wheelsets and rail, in which three DOFs are used to describe the movements of the bogie frame, i.e., the lateral displacement y_t, roll angle ϕ_t and yaw angle ψ_t, the remainders are used to describe the movements of three wheelsets, i.e., the lateral displacements y_{wi} and yaw angle $\psi_{wi}(i = 1, 2, 3)$. In the symbols y_{wi} and ψ_{wi}, the subscript $i = 1, 2, 3$ correspond to the leading, middle and trailing wheelsets of the locomotive bogie, respectively.

Considering the left-right symmetry and before-after symmetry of structure of the bogie system, the lateral hunting motion of the three-axle locomotive bogie system can be governed by the following equations

$$\begin{aligned}
m_w\ddot{y}_{wi} &= -F_{yfi} + F_{lyi} + F_{ryi} + N_{lyi} + N_{ryi} - F_t(y_{wi})\\
I_{wz}\ddot{\psi}_{wi} &= -b_1 F_{xfi} + b(F_{lxi} + N_{lxi} - F_{rxi} - N_{rxi})\\
&\quad + b\psi_{wi}(F_{lyi} + N_{lyi} - F_{ryi} - N_{ryi}) + M_{lzi} + M_{rzi} - I_{wy}\dot{\phi}_{wi}\Omega\\
m_t\ddot{y}_t &= -F_{yt} + F_{yf1} + F_{yf2} + F_{yf3}\\
I_{tz}\ddot{\psi}_t &= -b_2 F_{xt} + d_e F_{yt} + b_1(F_{xf1} + F_{xf2} + F_{xf3}) - (l_1 + d_e)F_{yf3}\\
&\quad - d_e F_{yf2} + (l_1 - d_e)F_{yf1}\\
I_{tx}\ddot{\phi}_t &= -b_1(F_{zf1} + F_{zf2} + F_{zf3}) - h_1(F_{yf1} + F_{yf2} + F_{yf3})\\
&\quad - b_2 F_{zt} - h_2 F_{yt}.
\end{aligned} \tag{10}$$

where M_t and m_w are the masses of the frame and wheelset of the bogie, respectively; I_{tx} and I_{tz} are the mass moments of inertia of the bogie frame about X-axis and Z-axis, respectively; I_{wy} and I_{wz} are the mass moments of inertia of the wheelset about Y-axis and Z-axis; d_e is the longitudinal distance from the mass center of the frame to the center line of the middle wheelset; h_1 is the distance from the mass center of the frame to the plane through the center lines of the leading, middle and trailing wheelsets, and h_2 is the distance from the mass center of the frame to the secondary lateral suspension.

Based on the relative lateral displacements, roll angles and yaw angles between the leading, middle and trailing wheelsets and the bogie frame, the longitudinal, lateral and vertical forces (F_{xfi}, F_{yfi} and F_{zfi}) at the primary suspension of the wheelsets are, respectively, given by

$$\begin{aligned}
F_{xfi} &= 2K_{px}b_1(\psi_{wi} - \psi_t) + 2C_{px}b_1(\dot{\psi}_{wi} - \dot{\psi}_t)\\
F_{yfi} &= 2K_{py}(y_{wi} - y_t \mp l_b\psi_t + h_1\phi_t) + 2C_{py}(\dot{y}_{wi} - \dot{y}_t \mp l_b\dot{\psi}_t + h_1\dot{\phi}_t)\\
F_{zfi} &= 2K_{pz}b_1(\phi_{wi} - \phi_t) + 2C_{pz}b_1(\dot{\phi}_{wi} - \dot{\phi}_t),
\end{aligned} \tag{11}$$

where the subscript $i = 1$, 2 and 3 in the physical quantities in the paper represents the leading, middle and trailing wheelsets of the bogie, respectively. The sign $\mp$ is taken upper '–' if $i = 1$, lower '+' if $i = 2$ and 3. $l_b = l_1 - d_e$, $l_b = d_e$ and $l_b = l_1 + d_e$ for $i = 1$, 2 and 3, respectively. According to the relative displacement, roll angle and yaw angle between the bogie frame and the car body, we can derive the longitudinal, lateral and vertical forces (F_{xt}, F_{yt} and F_{zt}) at the secondary suspension of the bogie, which are expressed as follows

$$\begin{aligned}
F_{xt} &= 2K_{sx}b_2\psi_t + 2C_{sx}b_2\dot{\psi}_t,\ F_{yt} = 2K_{sy}(y_t + h_2\phi_t) + 2C_{sy}(\dot{y}_t + h_2\dot{\phi}_t),\\
F_{zt} &= 2K_{sz}b_2\phi_t + 2C_{sz}b_2\dot{\phi}_t.
\end{aligned} \tag{12}$$

According to Eq. (10), the state vector of the three-axle locomotive bogie system can be written as

$$\begin{aligned}
\mathbf{Y}^{\mathrm{T}} = \{&\dot{y}_{w1}, \dot{y}_{w2}, \dot{y}_{w3}, \dot{\psi}_{w1}, \dot{\psi}_{w2}, \dot{\psi}_{w3}, \dot{y}_t, \dot{\psi}_t, \dot{\phi}_t, y_{w1}, y_{w2}, y_{w3},\\
&\psi_{w1}, \psi_{w2}, \psi_{w3}, y_t, \psi_t, \phi_t\}^{\mathrm{T}}.
\end{aligned} \tag{13}$$

the state space of the bogie system can be defined by $\mathbf{R}^{18} = \{Y | Y \in \mathbf{R}^{18}\}$.

2.4. Poincaré sections associated with the impacts between the leading, middle and trailing wheelsets and the rail

The steady-state solutions of Eq. (10) are relevant to the time t, the forward speed v and the initial conditions $\boldsymbol{Y}_0$. For some given speeds, there exist stationary or periodic solutions. Correspondingly, the locomotive bogie system exhibits the stationary and periodic hunting motions. The time response of the stationary motion, decaying to the vertical plane through the track centerline, corresponds to small forward speed v. When the forward speed v exceeds a critical speed, the stationary motion loses its stability and the periodic motions emerge. With progressive increase in v, the lateral displacements of the wheelsets gradually increase and finally exceed the flange clearance, and the lateral contacts between the wheel flange and the rail occur and lead to the impacts of the flange on the rail. According to Eq. (9), such impacts are referred to as soft impacts in the piecewise smooth dynamical systems [51–54]. The word 'soft' is used for describing the impact character between the wheel flange and the rail. Unlike the rigid impact described by the Newton elementary theory with coefficient of restitution, the duration of the soft impact is impossible to neglect. At some speed intervals, aperiodic hunting motion whose time response curve is irregular and seems like chaotic may also occur in the system. Therefore, we study dynamics of the locomotive bogie system with emphasis on the impact characteristics of the hunting motions and the incidence relation between the hunting types and dynamical parameters. Periodic or subharmonic-impact characteristics of the leading, middle and trailing wheelsets of the bogie system can be visually summarized by introducing the symbol n–p–q [55], where p and q refer to the number of impacts of some wheelset occurring on the left and right sides of the rail, respectively, and n represents the lateral cycle number associated with the frame center crossing the vertical plane through the track centerline in the positive direction of the y_{wi} coordinate.

The impact characteristic of the hunting motion of the bogie system can be studied by the Poincaré map. However, the definition of a Poincaré map needs to acknowledge the geometric structure of phase space of the dynamical system. So there actually is not a general method for the definition of Poincaré map. With regard to the illustration of different problems, the Poincaré maps of the bogie system, associated with the impacts of the leading, middle and trailing wheelsets on the rail, can be constructed in different ways by choosing correlative Poincaré sections

$$\sigma_{wi} = \left\{ (\boldsymbol{Y},\ v) \in \boldsymbol{R}^{18} \times \boldsymbol{V} \middle|\ y_{wi} = \eta,\quad \dot{y}_{wi} > 0;\quad y_{wi} = -\eta,\quad \dot{y}_{wi} < 0 \right\}, \tag{14}$$

$$\sigma_t = \left\{ (\boldsymbol{Y},\ v) \in \boldsymbol{R}^{18} \times \boldsymbol{V},\ \ y_t = 0,\ \ \dot{y}_t > 0 \right\}, \tag{15}$$

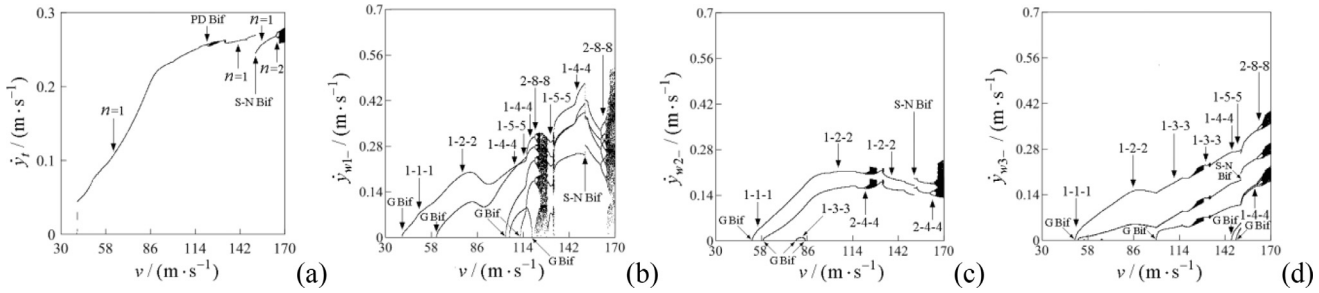

Fig. 3. Bifurcation diagrams of hunting motion of the locomotive bogie system ($\lambda = 0.056$): (a) $\dot{y}_t(v)$ corresponding to σ_t; (b) $\dot{y}_{w1-}(v)$ corresponding the right flange of the leading wheelset; (c) $\dot{y}_{w2-}(v)$ corresponding to the right flange of the middle wheelset; (d) $\dot{y}_{w3-}(v)$ corresponding to the right flange of the trailing wheelset.

where σ_{wi} ($i = 1, 2, 3$), respectively, correspond to the leading, middle and trailing wheelsets, $y_{wi} = \eta$ and $\dot{y}_{wi} > 0$ ($y_{wi} = -\eta$ and $\dot{y}_{wi} < 0$) aim at the condition under which the impacts occur at the right (left) side of the rail; σ_t corresponds to the bogie frame and both $y_t = 0$ and $\dot{y}_t > 0$ correspond to the condition under which the frame center is crossing the vertical plane through the track centerline in the positive direction of the y_t coordinate.

The feature extraction of the hunting motion of the bogie system can be numerically accomplished by the maps associated with the Poincaré sections (14) and (15). As expected, the impact number p and q of the hunting motion of the leading (middle or trailing) wheelset can be determined by the branch number of bifurcation diagram corresponding to σ_{w1} (σ_{w2} or σ_{w3}) and the lateral cycle number n of the locomotive bogie system can be ascertained by the branch number of bifurcation diagram related to σ_t.

3. Lateral hunting motions and bifurcation characteristics of the railway bogie system

The following research target and contents focus on lateral dynamics of the three-axle railway locomotive bogie with emphasis on further revealing what can happen for the railway vehicles running at speeds which are higher than the corresponding critical speeds, how strong the effect dynamical parameters on the hunting motions with the flange forces is, and which parameters have a significant influence on such hunting motions. Lateral hunting motions and bifurcation characteristics of the locomotive bogie system can be numerically analyzed by means of Eq. (10) and Poincaré sections specially defined by the formulas (14) and (15). Let us consider the basic parameters of spatial bogie model of a locomotive bogie:m_t = 24,373 kg, m_w = 3239 kg, $I_{tx} = 7475$ kg m^2, $I_{tz} = 52561$ kg m^2, $I_{wy} = 4051$ kg m^2, $I_{wz} = 2450$ kg m^2, $K_{px} = 4.113\times10^7$ N/m, $K_{py} = 5.2\times10^6$ N/m, $K_{pz} = 2.1\times10^6$ N/m, $C_{px} = 0$ N s/m, $C_{py} = 0$ N s/m, $C_{pz} = 5.0\times10^4$ N s/m, $K_{sx} = 1.2336\times10^5$ N/m, $K_{sy} = 5.36\times10^5$ N/m, $K_{sz} = 2.326\times10^6$ N/m, $C_{sx} = 0$ kN s/m, $C_{sy} = 9.0\times10^4$ N s/m, $C_{sz} = 9.0\times10^4$ N s/m, $b_1 = 1.025$ m, $b_2 = 1.025$ m, $l_1 = 2.15$ m, $h_1 = 0.032$ m, $h_2 = 0.478$ m, $r_0 = 0.625$ m, $\eta = 0.0091$ m, $b = 0.7465$ m, $\mu = 0.15$. Taking this set of parameters as the criterion parameters, we can extend the parameter space of the locomotive bogie so as to further uncover its dynamical behaviors from the multi-parameter views and the system levels. Therefore, we first need to understand and grasp dynamics of the locomotive bogie system with emphasis on hunting motion and bifurcations under the criterion parameter condition. Basic patterns, characteristics and diversity of hunting behaviors of the leading, middle and trailing wheelsets and the frame can be exactly extracted by quantitative datum from Poincaré sections σ_{wi} (i = 1, 2, 3) and σ_t chosen for the special purpose, respectively. Bifurcation diagrams of hunting motion of the locomotive bogie system, associated with the new wheelsets with the wheel tread's equivalent conicity $\lambda = 0.056$, are shown for the criterion parameters in Fig. 3. Local details of Fig. 3 are provided in Fig. 4, in which the symbols 'G Bif', 'PD Bif' and 'S-N Bif' represent grazing, period doubling and saddle-node bifurcations, respectively. Fig. 3(a) shows the bifurcation diagram $\dot{y}_t(v)$ which represents the velocity of the frame center crossing the vertical plane through the track centerline in the positive direction. Except chaotic hunting motion, the cycle numbers of hunting motion of the locomotive bogie, i.e., the hunting period number, can be determined by the branch number of the bifurcation diagram. The impact velocities of the leading, middle and trailing wheelsets on the rail are illustrated by the bifurcation diagrams versus to the forward speed v, as seen in Fig. 3(b)–(d). Except chaotic hunting motion, the impact numbers of the leading wheelset on the right side of rail, in a hunting period, can be determined by the branch number of the bifurcation diagram. From the bifurcation diagram shown in Fig. 3(b), we can observe that 1-1-1 hunting motion of the leading wheelset is derived from the non-smooth bifurcation of the hunting motion without impact (1-0-0 motion) induced by the symmetric grazing contracts between the left and right wheel flanges and the rail, i.e., grazing bifurcation (or grazing singularity of impact Poincaré map) [56]. The pioneer work in the grazing bifurcation was done by Nordmark [56], who studied analytically the occurrence and transition mechanism of grazing singularities in a piecewise linear system. Thereafter, this work has been further expanded by discontinuity-geometry approaches of maps to a series of piecewise smooth oscillators, where some geometric characteristics of grazing bifurcations of impact maps have been revealed [57–60]. Similarly, symmetric 1-2-2 motion is derived from the grazing bifurcation of symmetric 1-1-1 motion. At the running speed corresponding to grazing bifurcation, the flange of the leading wheelset, associated with 1-1-1 symmetric hunting motion, begins to touch the rail. It can be regarded as the 1-2-2 hunting motion, but the impact velocities of the additional left and right two impacts degenerate to touching. This means that a new hunting motion is characterized by 1-2-2, in which the velocities of pair of impacts occurring on the left and right sides of the rail increase gradually from zero with increasing the forward speed v. Subsequently, the transition from symmetric 1-2-2 to symmetric 1-5-5 hunting motion, caused by grazing bifurcations of symmetric 1-2-2, 1-3-3 and 1-4-4 hunting motions in sequence, occurs with increase in forward speed v, as seen in Fig. 3(b). Pitchfork bifurcation of symmetric 1-5-5 hunting motion occurs along with the increase of forward speed v. Consequently, asymmetric 1-5-5 hunting motion is created, two antisymmetric forms of which can exist in the dependence on the initial conditions of the locomotive bogie system. The complex transition from asymmetric 1-5-5 hunting motion to asymmetric 1-4-4 hunting motion occurs through a series of non-smooth bifurcations induced by asymmetric grazing contacts between the left and right wheel flanges and the rail, and for local details; see Fig. 4(a). Thereafter, 2-8-8 hunting motion stabilizes via period doubling bifurcation of asymmetric 1-4-4 motion. However, the branches of impact velocity of 2-8-8 hunting motion versus the forward speed v are nonsmooth or even discontinuous due to four grazing bifurcations supervening so that 2-7-8, 2-7-9 and 2-8-9 motion appear in sequence and 2-8-8 hunting motion finally arise again. The grazing bifurcation of 2-8-9 motion brings about that the impact velocity of one of nine impacts occurring on the right side of the rail degenerates to touching. Consequently, one impact of 2-8-9 motion

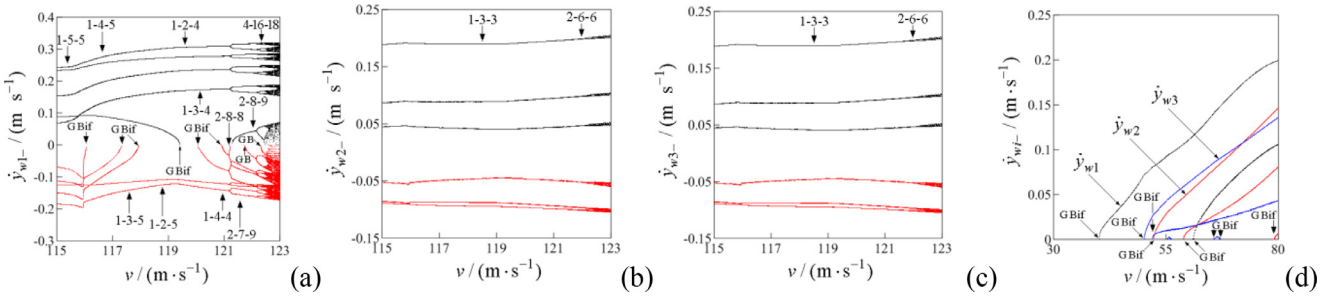

Fig. 4. Bifurcation diagrams of hunting motion of the locomotive bogie system: (a) detail of Fig. 3(b), $v \in [115, 123]$m/s; (b) detail of Fig. 3(c); (c) detail of Fig. 3(d); (d) grazing bifurcation diagrams $\dot{y}_{wi-}(v)$ of 1-0-0 motions of three wheelsets ($i = 1, 2, 3$), $v \in [30, 80]$m/s.

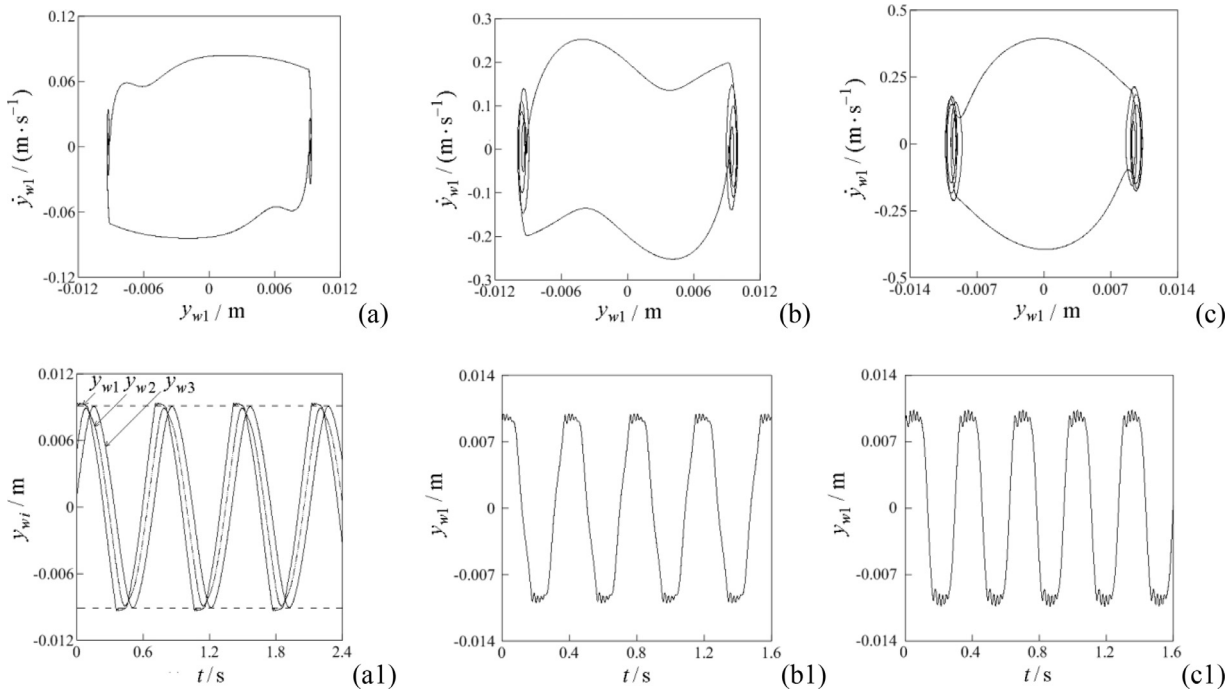

Fig. 5. Phase plane portraits and time series of the leading wheelset: (a) and (a1) 1-1-1 hunting motion, $v = 50$ m/s; (b) and (b1) 1-2-2 hunting motion, $v = 80$ m/s; (c) and (c1) 1-3-3 hunting motion, $v = 104.5$ m/s.

disappears and 2-8-8 hunting motion reappears. With in crease in v, the leading wheelset exhibits the standard period doubling route to chaos, starting from asymmetric 2-8-8 hunting motion. According to Figs. 3(b) and 4(a), the transition from symmetric 1-1-1 to chaotic hunting motion is briefly summarized by the following sequence: $v\uparrow$: 1-1-1_S → G Bif → 1-2-2_S → G Bif → 1-3-3_S → G Bif → 1-4-4_S → G Bif → 1-5-5_S → PF Bif → 1-5-5_{AS} → G Bif → 1-4-5 → G Bif → 1-3-5 → G Bif → 1-2-5 → G Bif → 1-2-4 → G Bif → 1-3-4 → G Bif → 1-4-4_{AS} → PD Bif → 2-8-8 → G Bif → 2-7-8 → G Bif → 2-7-9 → G Bif → 2-8-9 → G Bif → 2-8-8 → standard period doubling route to chaos. In the sequence, the symbol $v\uparrow$ denotes the increase of forward speed v; the subscript "S" and "AS" denote the symmetry and asymmetry, and G Bif, PF Bif and PD Bif represent grazing, pitchfork and period doubling bifurcations, respectively.

Phase plane portraits and time series of the leading wheelset are shown for $v = 50$, 80 and 106.5 m/s in Fig. 5. Phase plane portraits of more types of hunting motions, e.g., symmetric 1-4-4, asymmetric 1-5-5, 1-4-5, 1-3-5, 1-2-5, 1-2-4, 1-3-4, asymmetric 2-8-8 motions and etc., are shown for $v \in [97, 164.55]$m/s in Fig. 6. As shown in Figs. 3(b) and 4(a), the 1-2-2 hunting motion dominates in a wide range of running speed and the impact velocity of the hunting motion of the leading wheelset gradually become large along with increase of the forward speed v, starting from $v = 60.82$ m/s to its local upper bound $v = 80.96$ m/s. With increase in v, the impact velocity of 1-2-2 hunting motion reduces gradually until its local lower bound $v = 88.83$ m/s. Subsequently, the impact velocity of the motion increases gradually until the occurrence of grazing bifurcation of 1-2-2 hunting motion. It is found that the grazing bifurcations of 1-2-2 motions of the middle and trailing wheelsets have successively changed the variation tendency of impact velocity of 1-2-2 motion of the leading wheelset. It is important to note that the hunting motion of the leading wheelset successively goes through four grazing bifurcations which finally lead to the transition from hunting motion without impact to 1-5-5 hunting motion. The aforementioned hunting motions from 1-1-1 to 1-5-5 are of the symmetry in motion trajectories. Correspondingly, the grazing contacts between the left and right wheel flanges and the rail exhibit the symmetry. Pitchfork bifurcation of symmetric 1-5-5 hunting motion changes such symmetry due to the stabilization of asymmetric 1-5-5 motion. Thereafter, the grazing contacts between the left and right wheel flanges and the rail become also asymmetric. With increase in the forward speed v, a series of asymmetric grazing bifurcations occur and bring about 1-4-5, 1-3-5, 1-2-5, 1-2-4, 1-3-4, asymmetric 1-4-4, starting from asymmetric 1-5-5 motion, as seen in Figs. 4(a) and 6. Period doubling bifurcation of the asymmetric 1-4-4 motion occurs and asymmetric 2-8-8 motion stabilizes, but no period doubling sequence of the motion appears due to a series of grazing bifurcations until 2-8-8 motion is recreated, as mentioned above. Period doubling bifurcation of asymmetric 1-4-4 motion only changes

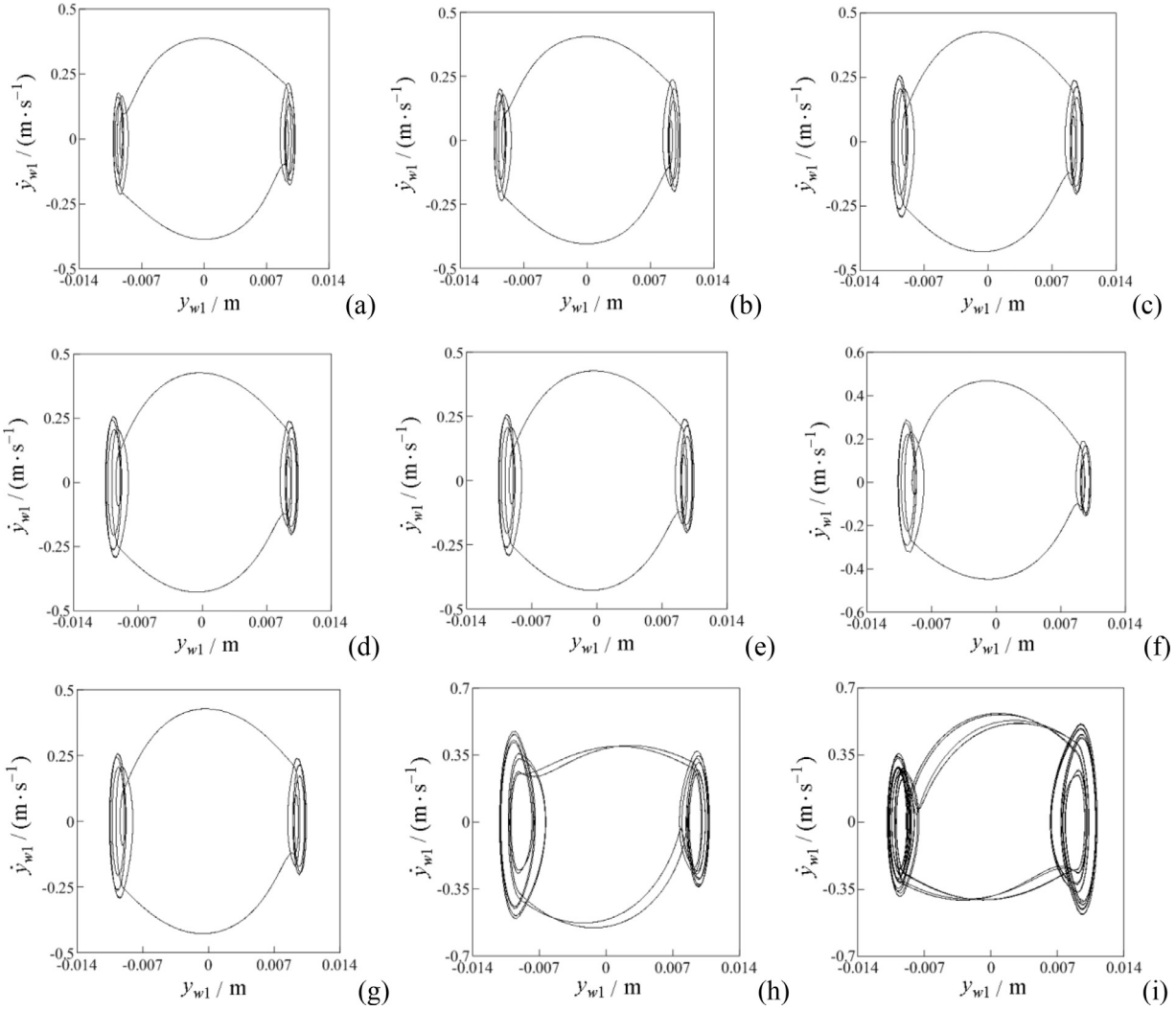

Fig. 6. Phase plane portraits of the leading wheelset: (a) 1-4-4 hunting motion, v = 97 m/s; (b) 1-5-5 hunting motion, v = 114 m/s; (c) 1-4-5 hunting motion, v = 116.5 m/s; (d) 1-3-5 hunting motion, v = 117.5 m/s; (e) 1-2-5 hunting motion, v = 118.5 m/s; (f) 1-2-4 hunting motion, v = 119.44 m/s; (g) 1-3-4 hunting motion, v = 120.5 m/s; (h) 2-8-8 hunting motion, v = 162.5 m/s; (i) 4-16-16 hunting motion, v = 164.55 m/s.

the period characteristic of hunting motion of the locomotive bogie system. However, grazing bifurcations occurring before the period doubling bifurcation influence the impact effect of three wheelsets on the rail. It is emphasized that the hunting motions without impact include the stationary hunting motion (SHM) and 1-0-0 motion. Such hunting motions without impact are marked with the symbol "SHM and 1-0-0″ in the parameter plane. The impacts of the middle and trailing wheelsets on the rail fall behind that of the leading wheelset, 1-2-2 hunting motion dominates for the middle wheelset, and 1-2-2 and 1-3-3 hunting motions dominate for the trailing wheelset due to fewer grazing bifurcations than those which the leading wheelset undergoes, as observed directly by comparing Fig. 3(b)–(d) and Fig. 4(d). The impact lag of the hunting motion of the middle wheelset is the most obvious of the three wheelsets. The phenomena can be observed by the phase plane portraits shown in Fig. 7. For example, the leading wheelset has exhibited 1-1-1 symmetric hunting motion at $v = 50$ m/s. However, the middle and trailing wheelsets still exhibit 1-0-0 hunting motions at the forward speed, for concrete details; see Fig. 7(a)–(c). Thereafter, the leading and trailing wheelsets are exhibiting 1-1-1 symmetric hunting motion at $v = 52$ m/s, and the middle wheelset is still in 1-0-0 motion, as seen in Fig. 7(d)–(f). Moreover, the top branch of impact velocity bifurcation diagram of the hunting motion of the trailing wheelset, associated with $n = 1$, is slightly lower than those of the leading and middle wheelset, as seen in Fig. 3(b)–(d). According to the details of bifurcations of hunting-impact motions of three wheelsets, we can find that the hunting-impact characteristics of the leading wheelset are more diverse and more complex than those of the middle and trailing wheelsets and non-smooth bifurcations induced by the grazing contacts between the wheel flange and the rail have the most important features in diversity and complexity of hunting motions. Hereinafter, Special attention will be paid to illustrating the hunting behaviors and bifurcation characteristics of the leading wheelset of the locomotive bogie. Figs. 8 and 9 are bifurcation diagrams of hunting motion of the locomotive bogie system associated with the worn wheelsets with the wheel tread's equivalent conicity $\lambda = 0.15$.

The schematic diagram shown in Fig. 1 is a lateral dynamic model of the three-axle bogie of a speed raising locomotive [43], which usually runs on straight track and curved tracks with large radius [43]. Therefore, the lateral stiffness of the leading, middle and trailing wheelsets is considered the same in Refs. [43,44]. If there are some curved tracks with small radius in the train running line, it should be considered to reduce the lateral stiffness of the middle wheelset of the three-axle locomotive bogie with respect to the one of the leading and trailing wheelsets for reducing the lateral forces when negotiating sharp curves. The lateral stiffness of the leading and trailing wheelsets is kept constant ($K_{py1} = K_{py2} = K_{py}$) and the lateral stiffness K_{py2} of the middle wheelset is reduced to $0.75K_{py}$, $0.5K_{py}$ and $0.25K_{py}$. Based on the criterion param-

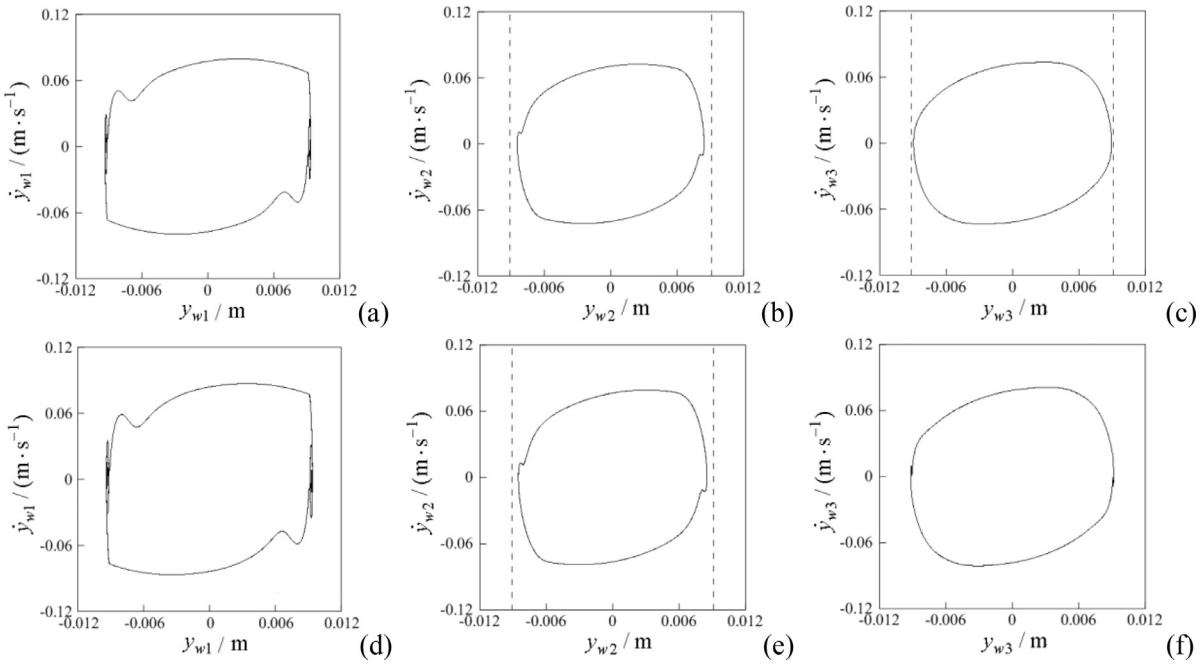

Fig. 7. Phase plane portraits of three wheelsets of the locomotive bogie: (a) 1-1-1 motion, leading wheelset, $v = 50$ m/s; (b) 1-0-0 motion, middle wheelset, $v = 50$ m/s; (c) 1-0-0 motion, trailing wheelset, $v = 50$ m/s; (d) 1-1-1 motion, leading wheelset, $v = 52$ m/s; (e) 1-0-0 motion, middle wheelset, $v = 52$ m/s; (f) 1-1-1 motion, trailing wheelset, $v = 52$ m/s.

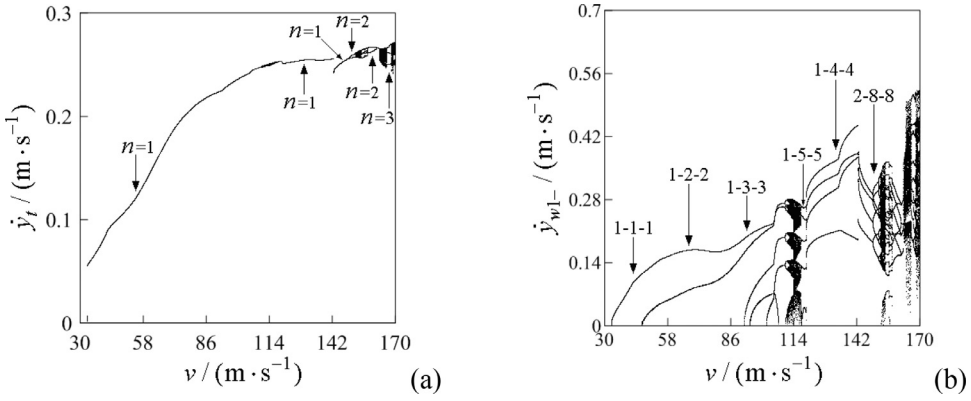

Fig. 8. Bifurcation diagrams of hunting motion of the locomotive bogie system ($\lambda = 0.15$): (a) $\dot{y}_t(v)$ corresponding to σ_t; (b) $\dot{y}_{w1-}(v)$ corresponding to σ_{w1}.

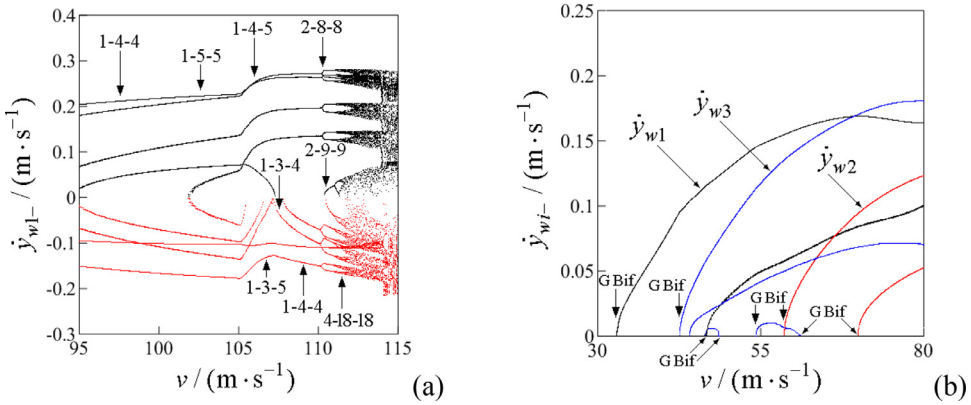

Fig. 9. Bifurcation diagrams of hunting motion of the leading wheelset of locomotive bogie: (a) detail of Fig.8(b), $v \in [95, 115]$m/s; (b) grazing bifurcation diagrams $\dot{y}_{wi}(v)$ of three wheelsets ($i = 1, 2, 3$), $v \in [30, 80]$m/s.

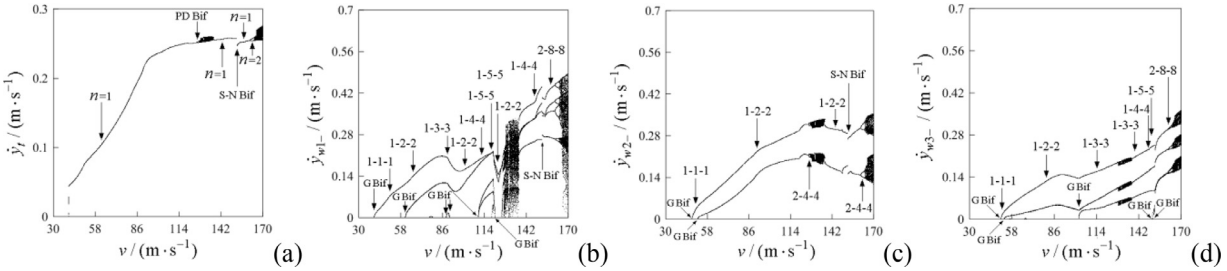

Fig. 10. Bifurcation diagrams of hunting motion of the locomotive bogie system with $K_{py1} = K_{py3} = K_{py}$, $K_{py2} = 0.5K_{py}$, $\lambda = 0.056$: (a) $\dot{y}_t(v)$ corresponding to σ_t; (b) $\dot{y}_{w1-}(v)$ corresponding the right flange of the leading wheelset; (c) $\dot{y}_{w2-}(v)$ corresponding to the right flange of the middle wheelset; (d) $\dot{y}_{w3-}(v)$ corresponding to the right flange of the trailing wheelset.

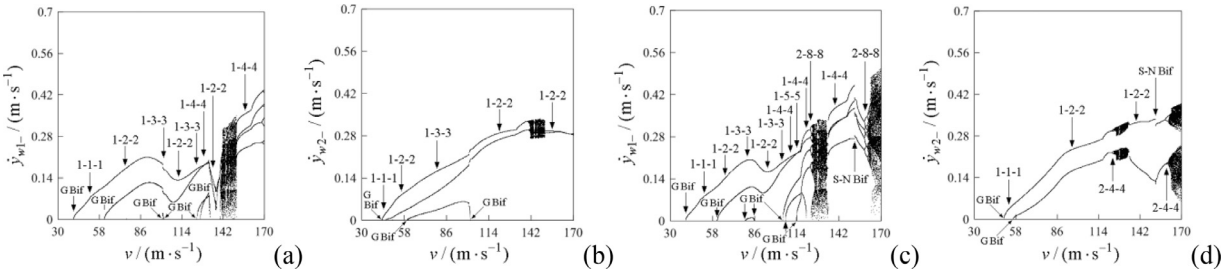

Fig. 11. Bifurcation diagrams of hunting motion of the locomotive bogie system with $K_{py1} = K_{py3} = K_{py}$ and $\lambda = 0.056$: (a) $\dot{y}_{w1-}(v)$ corresponding the right flange of the leading wheelset, $K_{py2} = 0.25K_{py}$ (b) $\dot{y}_{w2-}(v)$ corresponding to the right flange of the middle wheelset, $K_{py2} = 0.25K_{py}$; (c) $\dot{y}_{w1-}(v)$ corresponding the right flange of the leading wheelset, $K_{py2} = 0.75K_{py}$ (d) $\dot{y}_{w2-}(v)$ corresponding to the right flange of the middle wheelset, $K_{py2} = 0.75K_{py}$.

eters and the lateral stiffness reduction of the middle wheelset, hunting behaviors and bifurcations of the locomotive bogie system are numerically analyzed. The effects of lateral stiffness reduction of the middle wheelset on hunting behaviors of the locomotive bogie on straight track are presented for $K_{py2} = 0.5\ K_{py,}$ $0.25\ K_{py}$ and $0.75\ K_{py}$ in Figs. 10, 11(a) and (b), 11(c) and (d), respectively. Compared with Fig. 3, Fig. 10 and Fig. 11, we can find that the appropriate reduction of lateral stiffness of the middle wheelset has little effect on pattern types, conventional bifurcations and lateral impact velocity change of hunting behavior of the locomotive bogie. The reduction does not even affect the critical speeds related to grazing bifurcation of 1-0-0 motions of the leading and trailing wheelsets, but it can induce more grazing bifurcations of 1-2-2 motion and improve instability speed of period 1 hunting behavior of the bogie system. The reduction slightly decreases the critical speed related to grazing bifurcation of 1-0-0 motion of the middle wheelset and leads to a small increase in lateral impact velocity. As the reduction is large, for example $K_{py2} = 0.25\ K_{py}$, 1-3-3 motion induced by grazing bifurcation of 1-2-2 motion of the middle wheelset appears in the forward speed range $v \in [58, 101.2]$ m/s; see Fig. 11(b).

4. The incidence relation between lateral hunting patterns and system parameters

This section summarizes the correlative relationship between dynamics and key parameters, by which much information on hunting behaviors and bifurcation characteristics of the locomotive bogie system can be obtained. Hunting behaviors of the locomotive bogie system are governed by Eqs. (9) and (10) with more than 30 parameters, the non-smooth bifurcations of which result from the zero-velocity (or low-velocity) collision between the wheel flanges and the rail. Some key parameters influencing hunting patterns of the bogie system are considered with emphasis on K_{px}, K_{py}, λ, μ and v. The main concerns in the incidence relation are the numerical determinations of the occurrence regions, grazing and stability boundaries of various hunting motions of the three-axle railway locomotive bogie in the relevant parameter planes. The grazing instability of hunting motion, resulting in qualitative change of lateral dynamical properties of the bogie system, plays an important role in the occurrence of the hunting motions in the presence of the flange forces. Conventional bifurcation boundaries in the parameter planes, e.g., Period-doubling, saddle-node and Neimark–Sacker bifurcations, etc., are collectively referred to as stability boundaries, and non-smooth bifurcation boundary caused grazing contacts is described as grazing bifurcation boundary for the convenience of the following analysis. To simplify the presentation, periodic hunting motion of the locomotive bogie system, associated with the cycle number n, is defined as period n hunting motion. Correspondingly, the forward speed on the stability boundary of period n hunting motion is called instability speed of the periodic hunting motion. Real grazing bifurcations generally influence the numbers of impacts of three wheelsets on the rail, but it does not affect the current cycle specificity of the hunting motion of the bogie system. However, the stability bifurcation, whether period-doubling, saddle-node or Neimark–Sacker bifurcation, will not only change the original cycle characteristic of hunting motion of the bogie system, but also change the numbers of impacts of the wheelsets and the rail. Importantly, it is of practical value for dynamic design of the locomotive bogie to acquire the diversity and evolution of its hunting behaviors on the basis of the sampling ranges of these dynamical parameters extended from the criterion parameters. Taking the aforementioned basic parameters as the criterion parameters, we discuss the influence of key dynamical parameters, such as K_{px}, K_{py}, λ, μ, and v, on hunting diversity and evolution properties of the bogie system. The occurrence regions of various hunting motions of the leading, middle and trailing wheelsets, associated with the primary suspension lateral stiffness and the forward speed, can be numerically obtained by finely scanning the (v, K_{px}) parameter plane. The effects of changes in the lateral stiffness K_{py} are analyzed by comparing with the results associated with the criterion parameters. At the same parameter conditions, the basic characteristics of periodic hunting motions of three wheelsets are that the cycle number n is the same and the impact numbers may be different. The regions of various hunting motions ascertained by numerical analyses are marked with the symbol n–p–q and corresponding colors in Fig. 12. The periodic hunting motions unascertained, quasi-periodic and chaotic hunting motions are uniformly referred to the gray region in the parameter plane. The periodic hunting motions unascertained mean such motions whose cycle number n or impact number (p or q) in the hunting period is too big to be ascertained effectively. Based on

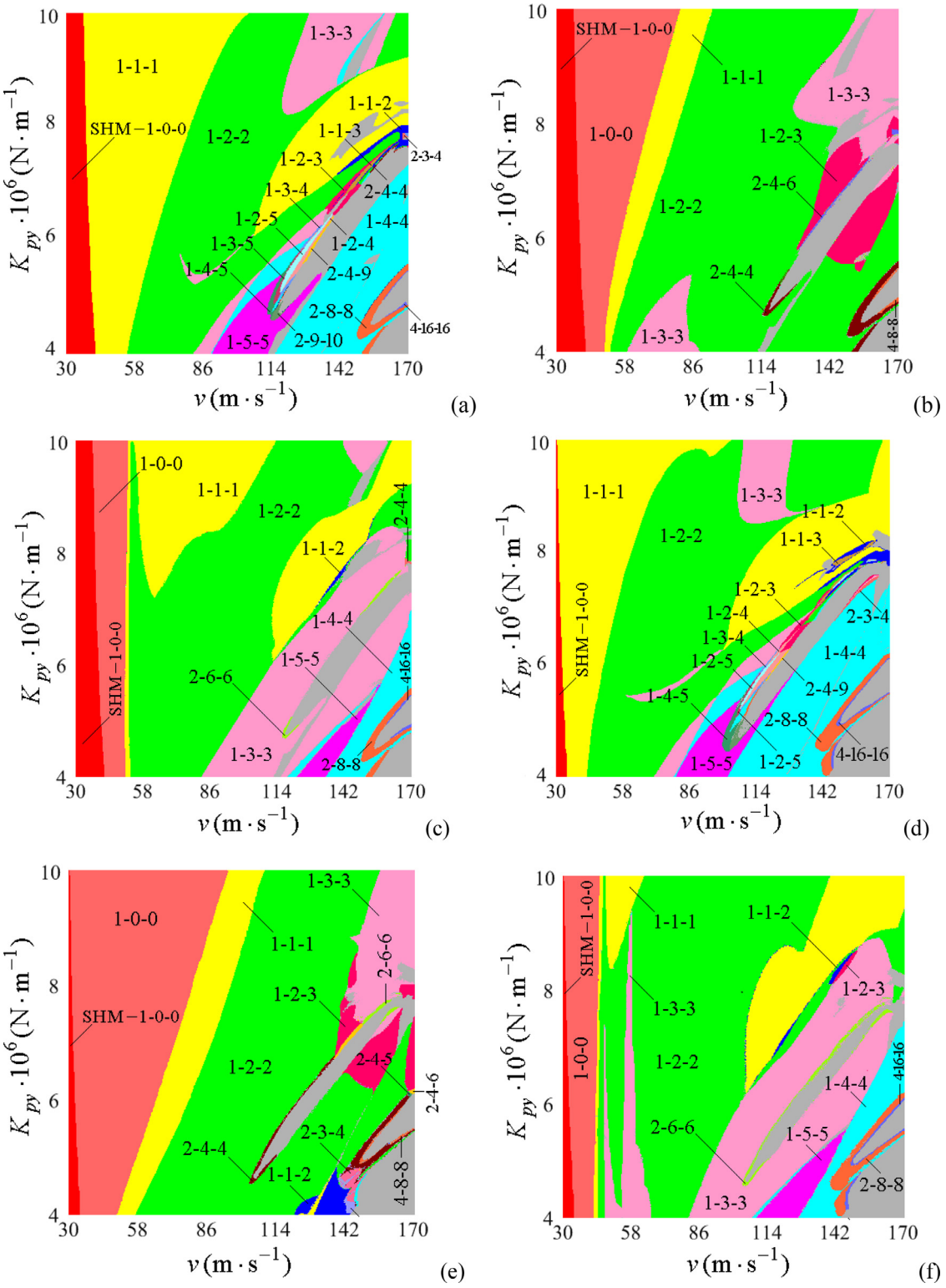

Fig. 12. Existence regions of various hunting motions of the leading, middle and trailing wheelsets in the (v, K_{py})–parameter plane: (a) leading wheelset with $\lambda = 0.056$; (b) middle wheelset with $\lambda = 0.056$; (c) trailing wheelset with $\lambda = 0.056$; (d) leading wheelset with $\lambda = 0.15$; (e) middle wheelset with $\lambda = 0.15$; (f) trailing wheelset with $\lambda = 0.15$.

the simulation results of the locomotive bogie system with the criterion parameters, the incidence relation between impact velocity and parameters (v, K_{px}) is analyzed. Diversity and qualitative properties of hunting motions, associated with the leading, middle and trailing wheelsets with the wheel tread's equivalent conicity $\lambda = 0.056$, can be graphically observed by Fig. 12(a)–(c) in sequence. In general, the wheel tread's equivalent conicity $\lambda = 0.056$ corresponds to the new wheelset without any wear, and $\lambda = 0.15$ is related to the wheelset with relative stable profile of wheel tread because of wears and tears. Some phenomena found under the criterion parameters are further observed. As seen in Fig. 12(a)–(c), the hunting-impact motions of the three wheelsets of the locomotive bogie system, related to $n = 1$, dominate in the parameter

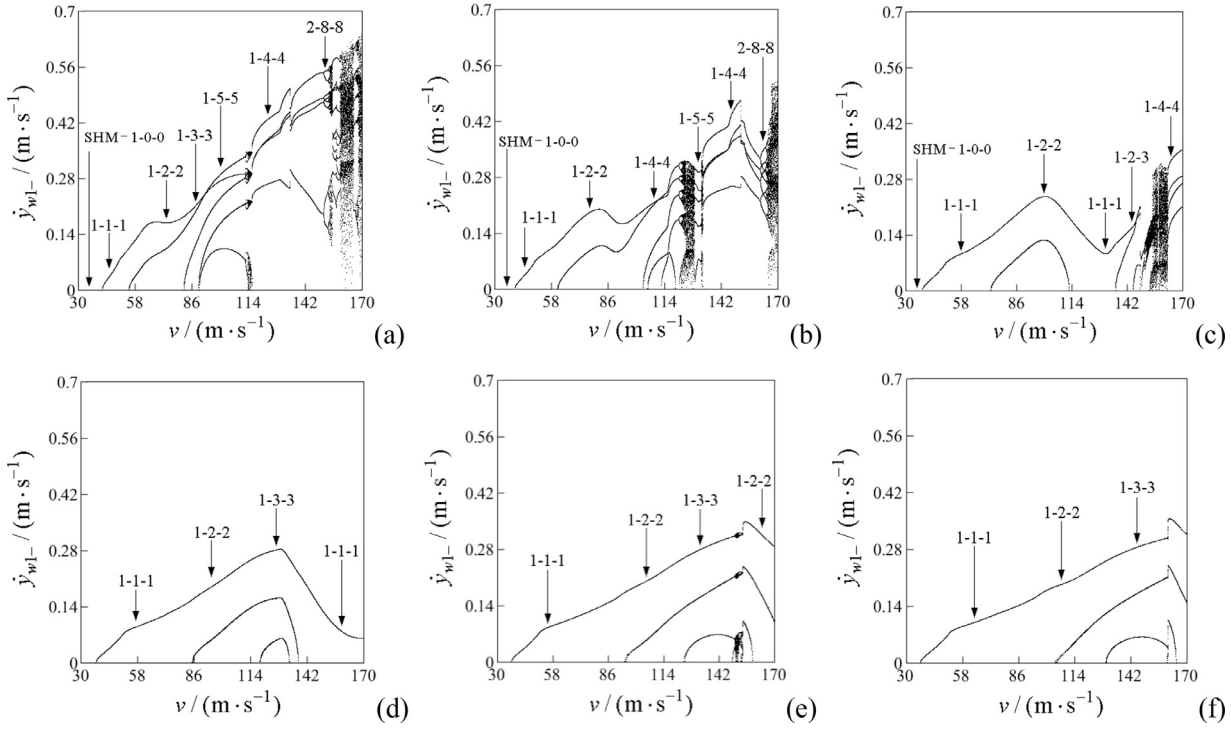

Fig. 13. Bifurcation diagrams of impact velocity of the leading wheelset, $\dot{y}_{w1-}(v)$, $\lambda = 0.056$: (a) $K_{py} = 4.0 \times 10^6$ N/m; (b) $K_{py} = 5.2 \times 10^6$ N/m; (c) $K_{py} = 7.0 \times 10^6$ N/m; (d) $K_{py} = 8.5 \times 10^6$ N/m; (e) $K_{py} = 9.4 \times 10^6$ N/m; (f) $K_{py} = 1.0 \times 10^7$ N/m.

plane and go through grazing, period doubling and saddle-node bifurcations; the impacts of the middle and trailing wheelsets on the rail obviously fall behind that of the leading wheelset; the occurrence region of 1-1-1 hunting motion of the middle wheelset is much smaller than that of the leading wheelset, and the occurrence region of 1-0-0 motion of the middle wheelset is much larger than that of the trailing wheelset. Diversity and complexity of hunting-impact characteristics of the locomotive bogie system are mainly distributed in parameter interval $K_{py} \in [4 \times 10^6, 8 \times 10^6]$N/m and are more clearly reflected in the leading wheelset. The hunting-impact patterns of the middle wheelset are relatively small and simple in comparison with those which the leading and trailing wheelsets exhibit in the same parameter interval. As shown in Fig. 12(b), 1-2-2 hunting motion dominates for the middle wheelset in the (v, K_{py})-parameter plane. The occurrence regions of 1-1-1 motion of the leading and trailing wheelsets are respectively segregated into two and three blocks by the existence domain of 1-2-2 motion due to grazing bifurcations of these two hunting motions. As for the trailing wheelset, the first region of 1-1-1 motion is extremely narrow and the grazing bifurcation boundary of the second region of 1-1-1 motion is very high. It can be said that the railing wheelset hardly shows the effect of 1-1-1 motion for $K_{py} \in [4 \times 10^6, 6 \times 10^6]$N/m, but the hunting motion is necessary for the formation of 1-2-2 motion; see Fig. 12(c). However, 1-1-1 motion of the middle wheelset can only occur in a narrow banded region sandwiched between two grazing boundaries related to 1-0-0 and 1-2-2 domains. As we known, there exist generally a cluster of grazing bifurcation boundaries which are located on the left of a stability boundary in the parameter plane. The stability bifurcation boundary will influence the periodic-hunting characteristic of the locomotive bogie system, including the cycle number n and the impact numbers p and q. Those grazing bifurcation boundaries represent the changes of the wheel–rail impact characteristics associated with the same hunting period. The cycle number of hunting motion of the locomotive bogie system will be changed crossing the stability boundary. The impact numbers of the leading, middle and trailing wheelsets on the rail are consistently changed after crossing these grazing bifurcation boundaries.

Bifurcation diagrams of impact velocity of the leading wheelset versus the forward speed v, extracted from Fig. 12(a) for $K_{py} = 4.0$, 5.2, 7.0, 8.5, 9.4, 10.0 MN/m, are shown in Fig. 13(a)–(f) in the form of $\dot{y}_{w1-}(v)$, respectively. The bifurcation diagram is useful when the wheel-rail impact velocity is of interest over the whole (v, K_{py}) – plane.

Existence regions of various hunting motions, associated with the leading, middle and trailing wheelsets with worn profile tread, are shown for the (v, K_{py})–parameter plane in Fig. 12(d)–(f), respectively. As for the worn wheelset with $\lambda = 0.15$, hunting patterns and distribution regularities, in the parameter plane, are basically similar to those related to the new wheelset with $\lambda = 0.056$; see bifurcation diagrams shown in Fig. 14. As for the bogie system with the worn wheelsets, the difference is that the stability boundary of period 1 hunting motion is generally on the left of that corresponding to the new wheelsets. Similar phenomena can also be observed in the (v, K_{px}), (v, μ) and (v, λ)–parameter planes, as seen in Figs. 15, 17 and 19. As for the trailing wheelset with worn profile tread, the occurrence region of the 1-1-1 motion becomes smaller due to the extension of the occurrence regions of 1-2-2 and 1-3-3 motions; see Fig. 12(d).

The occurrence regions of different types of hunting motions for the leading, middle and trailing wheelsets with variation of primary suspension longitudinal stiffness K_{px} and forward speed v are shown in Fig. 15(a) and (b), respectively. The former corresponds to the new wheelset without any wear, and the latter to wheelset with the worn profile tread. The effects of changes in the longitudinal stiffness K_{px} are analyzed by comparing with the results based on the criterion parameters. As for the periodic hunting motions, the leading, middle and trailing wheelsets have the same cycle number n at the same parameter conditions, but the impact numbers may be different in the hunting period, as shown in Fig. 15(a) and (b). The bogie system has a large occurrence region of hunting motion related to $n = 1$ in the parameter interval $K_{px} \in [2,10]$ MN/m, i.e., 1-p-p motions dominate in the (v, K_{px})–parameter plane. Different from the primary suspension lateral stiffness K_{py}, the influence of the change of longitudinal stiffness K_{px} on the hunting patterns is not obvious in the parameter interval $K_{px} \in [2,10]$ MN/m. As

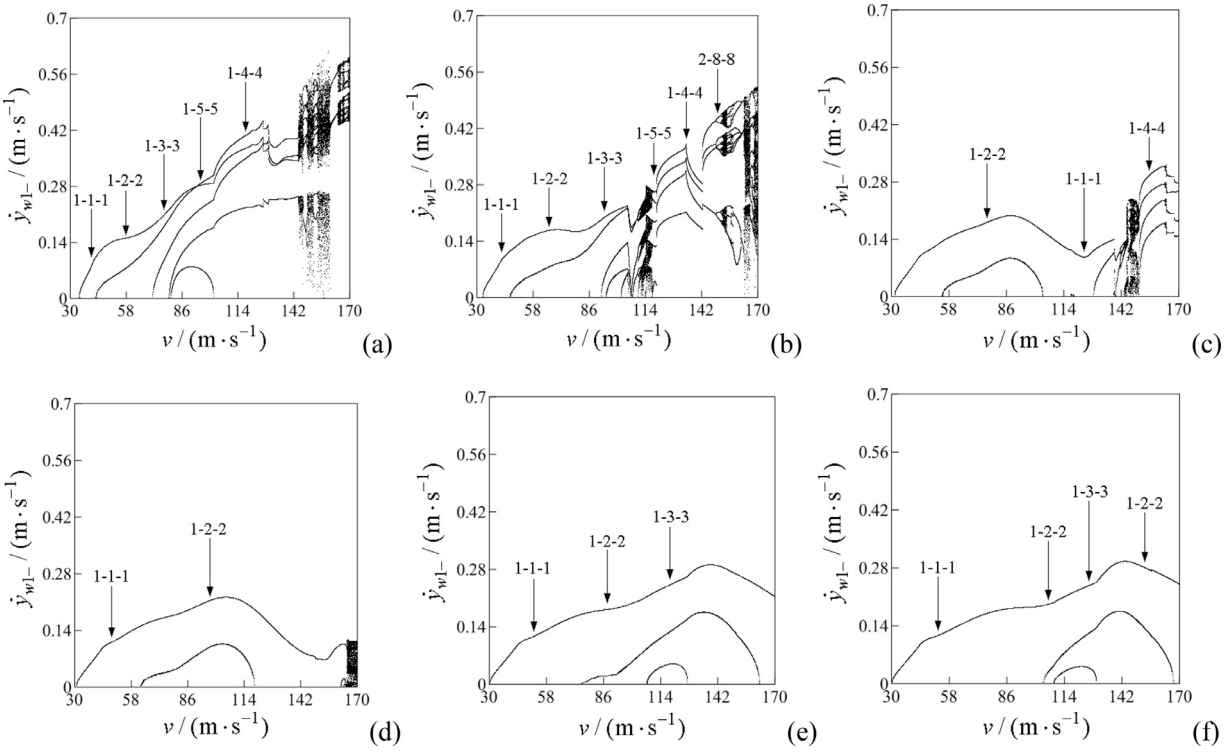

Fig. 14. Bifurcation diagrams of impact velocity of the leading wheelset, $\dot{y}_{w1-}(v)$, λ = 0.15: (a) K_{py} = 4.0 × 10^6 N/m; (b) K_{py} = 5.2 × 10^6 N/m; (c) K_{py} = 7.0 × 10^6 N/m; (d) K_{py} = 8.2 × 10^6 N/m; (e) K_{py} = 9.4 × 10^6 N/m; (f) K_{py} = 1.0 × 10^7 N/m.

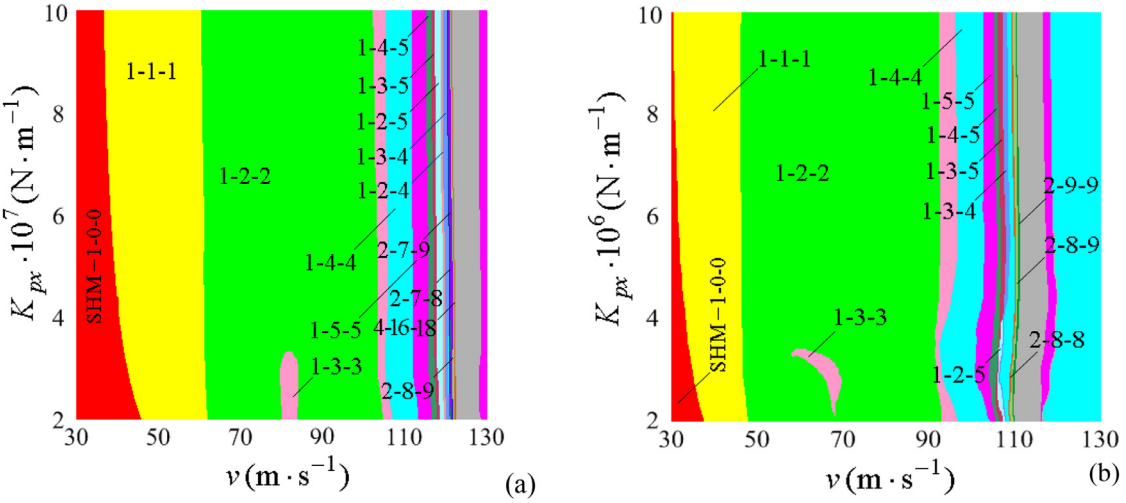

Fig. 15. Existence regions of various hunting motions of the leading wheelset in the (v, K_{px})–parameter plane: (a) λ = 0.056; (b) λ = 0.15.

shown in Fig. 15, the hunting patterns and characteristic regularities, in the (v, K_{px})–parameter plane, can be summarized: the increase of the forward speed v brings about a series of grazing bifurcations which realize the transition from symmetric 1-1-1 to symmetric 1-5-5 hunting motion; the occurrence region of symmetric 1-2-2 motion is the largest among 1-p-p motions ($p \geq 1$); a series of asymmetric grazing contacts between the wheel flange and the rail lead to 1-p-q motions, starting from asymmetric 1-5-5 motion caused by pitchfork bifurcation; the stability boundary of period 1 hunting motion of the bogie system, associated with the worn wheelsets, is obviously at the left of that corresponding to the new wheelsets. Bifurcation diagrams of impact velocity of the leading wheelset versus the forward speed v, extracted from Fig. 15(a), are shown for a few representative values of the primary suspension longitudinal stiffness K_{px} in Fig. 16. Different from the primary suspension lateral stiffness K_{py}, the variation of the longitudinal stiffness K_{px} has little effect on the branches of impact velocity bifurcation diagram of period 1 hunting motion of the leading wheelset.

The influence of the wheel–rail friction coefficient μ on dynamics of the locomotive bogie system is analyzed to epitomize the diversity and bifurcation characteristics of hunting motions. In Fig. 17(a) and (b) are plotted the occurrence regions of various hunting motions for the leading wheelsets with variation of the friction coefficient μ and the forward speed v. The former corresponds to the new wheelset with λ = 0.056 and the latter to worn wheelset with λ = 0.15. Bifurcation diagrams of impact velocity $\dot{y}_{w1-}$, associated with the new leading wheelset, are shown for six representative values extracted from the interval $\mu \in$ [0.1, 0.3] in Fig. 18. These bifurcation diagrams allow us to discover the regularity that the top branch of impact velocity bifurcation diagram of period

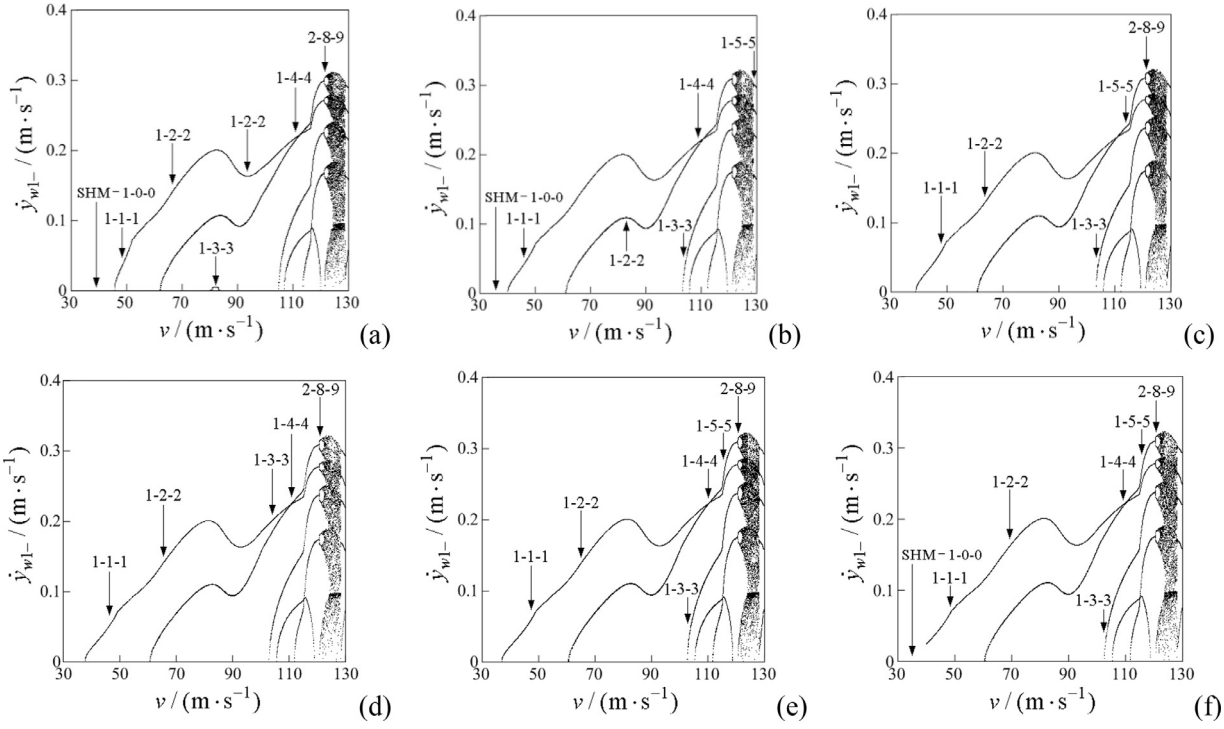

Fig. 16. Bifurcation diagrams of impact velocity of the leading wheelset, $\dot{y}_{w1-}(v)$, $\lambda = 0.056$: (a) $K_{px} = 2.0\times10^7$ N/m; (b) $K_{px} = 4.113\times10^7$ N/m; (c) $K_{px} = 5.2\times10^7$ N/m; (d) $K_{px} = 6.8\times10^7$ N/m; (e) $K_{px} = 8.5\times10^7$ N/m; (f) $K_{px} = 1.0\times10^8$ N/m.

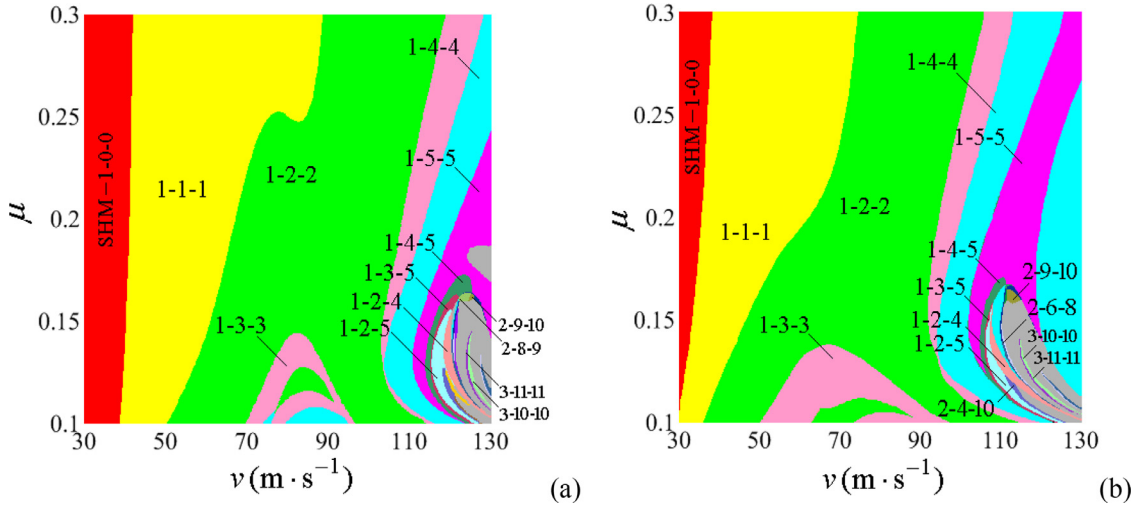

Fig. 17. Existence regions of various hunting motions of the leading wheelset in the (v, μ)–parameter plane: (a) $\lambda = 0.056$; (b) $\lambda = 0.15$.

1 hunting motion of the leading wheelset rises gradually with the increase of friction coefficient μ. However, this change is obvious only if the friction coefficient μ is greater than 0.15. The friction coefficient is related to the creep force, so it influences one of two key nonlinear factors of the locomotive bogie system, i.e., the creep force and the flange clearance. To some extent its change will more easily affect the hunting patterns. Near μ=0.1, the occurrence region of 1-2-2 hunting motion of the leading wheelset is isolated to three by a region including the 1-3-3 and 1-4-4 hunting motions. As for $\mu \in [0.1, 0.1626]$, a series of grazing bifurcations induce the transition from 1-0-0 to symmetric 1-5-5 motion with increase in the forward speed v; next, pitchfork bifurcation causes asymmetric 1-5-5 motion to stabilize; thereafter, the grazing contacts of the wheel flange and rail correspondingly exhibit the asymmetry and induce 1-4-5, 1-3-5, 1-2-5, 1-2-4, 1-3-4 motions in sequence; the leading wheelset finally falls into chaotic hunting motion via period doubling sequences of 1-2-5 or 1-3-4 motion; there exist narrow windows 2-8-9, 2-9-10, 3-10-10 and 3-11-11 motions mingled with chaotic domains. As for $\mu > 0.1626$, the leading wheelset mainly exhibits stationary hunting motion and 1-p-p motions (p = 0–5). On the whole, the hunting motions of the locomotive bogie system, associated with the cycle number $n = 1$, dominate in the parameter plane. The occurrence regions of chaotic motion and hunting motions with the cycle number larger than 1 are far less than that of hunting motions with the cycle number $n = 1$, and focus on a small tongue-shaped region in the lower right corner of Fig. 17(a). As for the worn leading wheelset with $\lambda = 0.15$, hunting patterns and distribution regularities, in the parameter plane, are basically similar to those related to the new wheelset with $\lambda = 0.056$. In general, the only difference is that the stability boundary of period 1 hunting motion, associated with the worn wheelsets, is slightly more left than that corresponding to the new wheelsets.

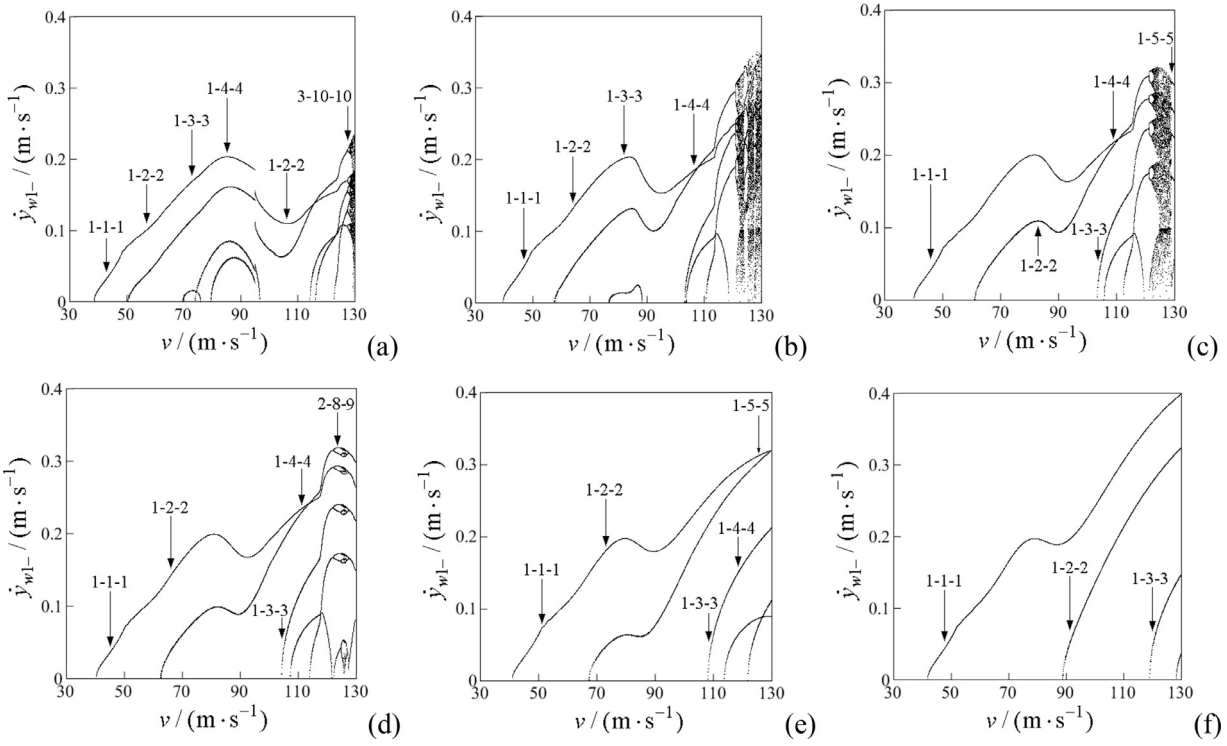

Fig. 18. Bifurcation diagrams of impact velocity of the leading wheelset, $\dot{y}_{w1-}(v)$, $\lambda = 0.056$: (a) $\mu = 0.1$; (b) $\mu = 0.13$; (c) $\mu = 0.15$; (d) $\mu = 0.16$; (e) $\mu = 0.2$; (f) $\mu = 0.3$.

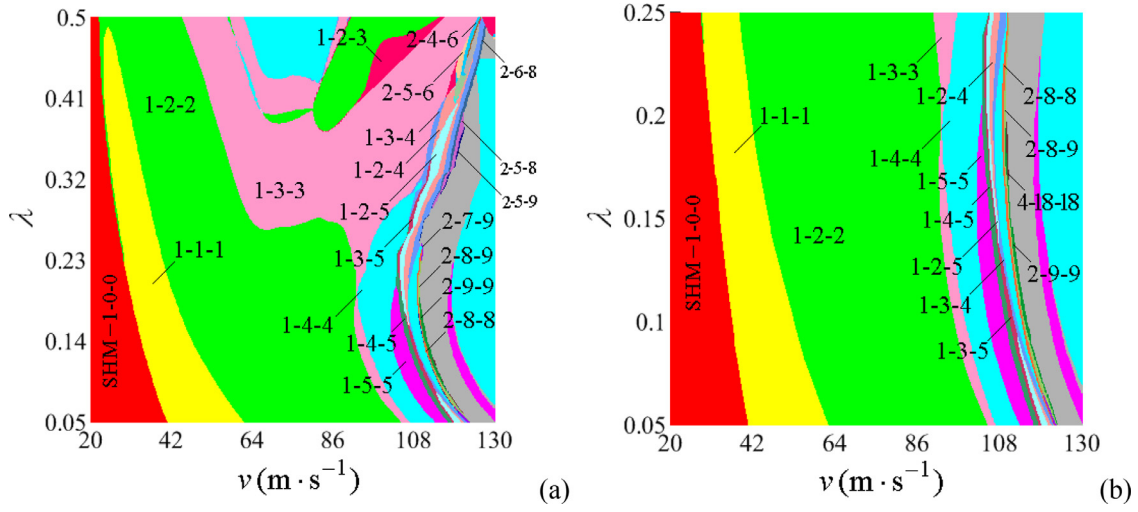

Fig. 19. Existence regions of various hunting motions of the leading wheelset in the (v, λ)–parameter plane: (b) details of Fig. 19(a).

As for the new wheelset without any wear, its wheel tread's equivalent conicity is 0.056. During the course of vehicle operation, the equivalent conicity of the wheel tread gradually becomes large with the abrasion of the wheelset on the rail. The hunting patterns and distributions associated with the (v, λ)-parameter plane are provided in Fig. 19, which illustrates the influences of the profile change of the wheel tread caused by the abrasion on the hunting patterns and bifurcation characteristics of the locomotive bogie system. Bifurcation diagrams of impact velocity $\dot{y}_{w1-}$ are shown for six representative values extracted from the interval $\lambda \in [0.05, 0.25]$ in Fig. 20. As shown in Figs. 19 and 20, small equivalent conicity λ brings about larger occurrence regions of period 1 hunting motions and slightly larger impact velocity of the leading wheelset on the rail than large λ. This means that the stability boundary of periodic hunting motion of the bogie system with worn wheelsets, associated with $n = 1$, is more left than that with new wheelsets and the top branch of impact velocity bifurcation diagram of period 1 hunting motion of the worn wheelset is slightly reduced on the whole with increase of λ. It is important to note that the change of the equivalent conicity λ has little influence on the instability speed of period 1 hunting motion of the locomotive bogie system and the top branch of impact velocity of the hunting motion for $\lambda \in [0.15, 0.25]$; see Fig. 19(b) and Fig. 20(d)–(f). Also, the occurrence region of 1-2-2 motion in the (v, λ)-parameter plane is the largest among all hunting motions associated with the cycle number $n = 1$ for $\lambda \in [0.05, 0.25]$, the occurrence regions of other symmetric 1-p-p ($p > 2$) and asymmetric 1-p-q motions are very narrow. With increase in λ, the stability boundary of hunting motion, associated with the cycle number $n = 1$, reduces gradually until its lower bound $v_c = 110.2$ m/s at $\lambda = 0.2063$. As for $\lambda > 0.2063$, the stability boundary of period 1 hunting motion of the locomotive bogie system is gradually shifted to the right with increase in λ., and the occurrence region of

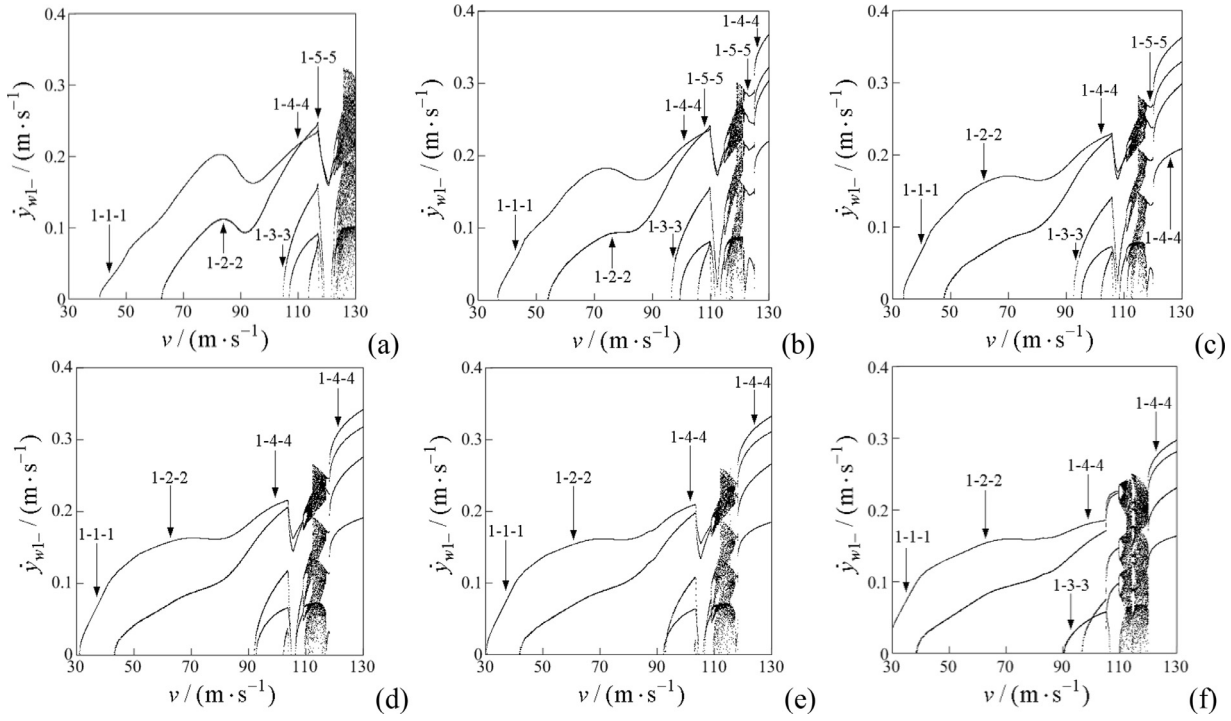

Fig. 20. Bifurcation diagrams of impact velocity of the leading wheelset, $\dot{y}_{w1-}(v)$: (a) $\lambda = 0.05$; (b) $\lambda = 0.095$; (c) $\lambda = 0.14$; (d) $\lambda = 0.185$; (e) $\lambda = 0.2$; (f) $\lambda = 0.25$.

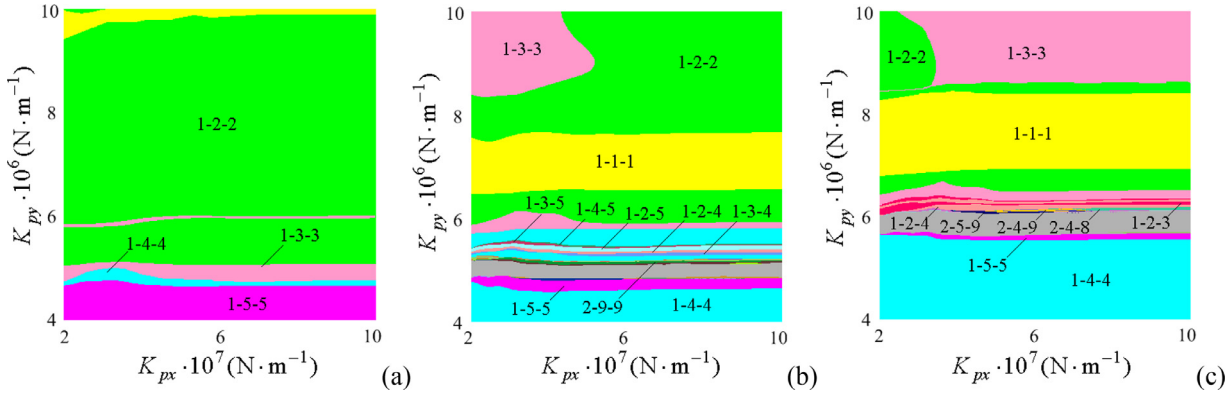

Fig. 21. Existence regions of various hunting motions of the leading wheelset in the (K_{px}, K_{py})–parameter plane: (a)$v = 90$ m/s; (b) $v = 110$ m/s; (c) $v = 125$ m/s.

1-3-3 motion becomes significantly larger so as to shrink the existence region of 1-2-2 motion.

As for a certain forward speed, the occurrence regions and grazing and stability boundaries of various hunting motions of the locomotive bogie system with the worn wheelsets, associated with variation of primary suspension parameters (e.g., K_{px} and K_{py}), can be numerically obtained by finely scanning the (K_{px}, K_{py})–parameter plane. The incidence relation between hunting patterns and primary suspension parameters (K_{px}, K_{py}) can provide a practical and convenient method for designing the desired instability speed of period 1 hunting motion of the bogie system and the optimal matching of its primary suspension parameters K_{px} and K_{py}. First, an estimated instability speed of periodic hunting behavior of the locomotive bogie system, associated with $n = 1$, is confirmed; secondly, taking a forward speed near the estimated instability speed as the reference, the hunting patterns and occurrence regions covering in the (K_{px}, K_{py})–parameter plane can be numerically computed; subsequently, the reasonable matching of primary suspension stiffness K_{px} and K_{py} can be preliminarily obtained according to the design requirement and the parameter region in which period 1 hunting motion dominates; a new estimated instability speed closer to the desired value is obtained and a repeat of the above process begins again. Based on the hunting patterns and occurrence regions over the (K_{px}, K_{py})–parameter plane associated with a series of estimated instability speeds, we can finally design a higher and desired instability speed of period 1 hunting motion of the bogie system with the reasonable matching of primary suspension parameters. The hunting patterns and occurrence regions of the leading wheelset of the bogie system, associated with the primary suspension parameters K_{px} and K_{py}, are illustrated for several representative forward speeds in Fig. 21(a)–(c), e.g., v = 90, 110 and 125 m/s, respectively. A stiffness matching range of the primary suspension, $K_{px} \in$ [18,22]MN/m and $K_{py} \in$ [6, 6.5]MN/m are obtained by the above mentioned method, which brings about a higher instability speed of period 1 hunting behavior. Partial bifurcation diagrams of impact velocity of the leading wheelset versus forward speed v, associated with $K_{px} \in$ [18,22]MN/m and $K_{py} \in$ [6, 6.5]MN/m and the remaining criterion parameters except K_{px} and K_{py}, are shown in Fig. 22, and the first two and the last two correspond to the new wheelset and the worn wheelset, respectively. Comparing with the hunting characteristics shown in Figs. 3(b) and 10(a), we can find that the instability speeds of period 1 hunting motions related to Fig. 22(a) and (b) and Fig. 22(c)

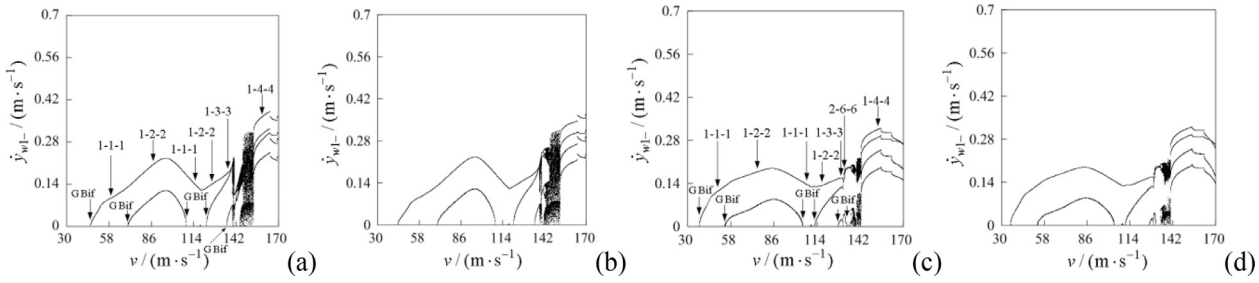

Fig. 22. Bifurcation diagrams of hunting motion of the leading wheelset of the bogie system: (a) K_{px} = 18 MN/m, K_{py} = 6.5 MN/m, λ = 0.056; (b) K_{px} = 22 MN/m, K_{py} = 6.5 MN/m, λ = 0.056; (c) K_{px} = 18 MN/m, K_{py} = 6.5 MN/m, λ = 0.15; (d) K_{px} = 22 MN/m, K_{py} = 6.5 MN/m, λ = 0.15.

and (d) are larger and the top branches of impact velocity bifurcation diagram of the leading wheelset, associated with $n = 1$, are slightly elevated.

5. Conclusions

This paper presents pattern diversity and bifurcation characteristics of hunting behaviors of a three-axle railway locomotive bogie in the presence of the flange contact nonlinearity. The leading wheelset successively goes through non-smooth bifurcations induced by symmetric grazing contacts of the wheel flanges and the rail with increase in forward speed, which lead to the transition from non-impact hunting motion to period-1 hunting motion with bilaterally symmetric and multi-impact characteristic. However, the symmetry-breaking of hunting behavior of the bogie system through a pitchfork bifurcation leads to asymmetric hunting motions in the railway bogie system. With further increase in forward speed, a series of grazing contacts between the left and right wheel flanges and the rail occur in succession and all hunting motions exhibit the asymmetry. The impacts of the middle and trailing wheelsets on the rail fall behind that of the leading wheelset, and the impact lag of the hunting motion of the middle wheelset is the most obvious of the three wheelsets. The impact number of the middle wheelset on the rail, in the hunting period, is likely to be less than that of the leading and trailing wheelsets due to less grazing contacts. The top branch of impact velocity bifurcation diagram of the hunting motion of the trailing wheelset, associated with $n = 1$, is slightly lower than those of the leading and middle wheelset. The hunting-impact characteristics of the leading wheelset are more diverse and more complex than those of the middle and trailing wheelsets.

The influences of the profile change of the wheel tread caused by the abrasion on the hunting patterns and bifurcation characteristics of the bogie system are investigated by finely scanning the parameter plane associated with the forward speed v and the equivalent conicity λ of wheel tread. The instability speed of period 1 hunting motion of the bogie system with worn wheelsets is lower than that with new wheelsets and the top branch of impact velocity bifurcation diagram of period 1 hunting motion of the worn wheelset is slightly lower than that of the new wheelset on the whole. In the (v, K_{py}), (v, K_{px}) and (v, μ)–parameter planes, the occurrence regions of hunting-impact motions of the bogie system with new wheelsets, associated with the cycle number $n = 1$, are slightly larger than those with worn wheelsets. The change of the primary suspension longitudinal stiffness has little effect on the hunting patterns of the locomotive bogie system with the worn wheelsets, and the increase of K_{px} brings about the slight increase of instability velocity caused by period doubling bifurcation of hunting motion associated with the cycle number $n = 1$. As for the same forward speed, the change of K_{px} has little effect on the impact velocity of period 1 hunting motion of the leading wheelset. Diversity and complexity of hunting-impact characteristics of the locomotive bogie system are mainly distributed in parameter interval $K_{py} \in [4 \times 10^6, 8 \times 10^6]$N/m and are more clearly reflected in the leading wheelset. Large occurrence region of hunting motion, associated with the cycle number $n = 1$, exists in the (v, K_{py})–parameter plane for $K_{py} \in$ [8.23, 10] MN/m. The change of wheel-rail friction coefficient μ has little effect on the hunting patterns of the bogie system. The top branch of impact velocity bifurcation diagram of period 1 hunting motion of the leading wheelset rises gradually with the increase of friction coefficient μ. However, this change is obvious only if the friction coefficient μ is greater than 0.15. Aimed at a series of estimated instability speeds of period 1 hunting motion and based on the hunting patterns and occurrence regions in the primary suspension parameter planes, a higher instability speed of period 1 hunting motion of the locomotive bogie system, associated with the matching range of primary suspension parameters, can be obtained. The stiffness matching of the primary suspension, $K_{px} \in$ [18,22] MN/m and $K_{py} \in$ [6, 6.5]MN/m, is presented, which brings about the increase of the instability speed and the slight increase of lateral impact velocity.

Acknowledgments

The authors gratefully acknowledge the support by National Natural Science Foundation of China (11362008, 11462012, 11672121) and Innovation and Entrepreneurship Talent Training Project in Lanzhou, China (2014-RC-33).

References

[1] Cooperrider NK. The hunting behavior of conventional railway trucks. J Eng Ind 1972;94(2):752–62.
[2] Nó M, Hedrick JK. High speed stability for rail vehicles considering varying conicity and creep coefficients. Veh Syst Dyn 1984;13:299–313.
[3] Kaas-Petersen C. Chaos in a railway bogie. Acta Mech 1986;61(1–4):89–107.
[4] Kaas-Petersen C, True H. Periodic, biperiodic and chaotic dynamical behavior of railway vehicles. Veh Syst Dyn 1986;15(6):208–21.
[5] True H. Railway vehicle chaos and asymmetric hunting. Veh Syst Dyn 1992;20(Sup1):625–37.
[6] Jensen CN, Golubitsky M, True H. Symmetry generic bifurcations, and mode interaction in nonlinear railway dynamics. Int J Bifurc Chaos 1999;9(7):1321–31.
[7] True H, Jensen JC. Parameter study of hunting and chaos in railway vehicle dynamics. Veh Syst Dyn 1994;23:508–21.
[8] True H. On the theory of nonlinear dynamics and its applications in vehicle systems dynamics. Veh Syst Dyn 1999;31(5–6):393–421.
[9] Zeng J. Numerical computations of the hunting bifurcation and limit cycles for railway vehicle system. J. China Railw Soc 1996;15(3):13–18.
[10] Ahmadian M, Yang SP. Effect of system nonlinearities on locomotive bogie hunting stability. Veh Syst Dyn 1998;29(6):365–84.
[11] Ahmadian M, Yang SP. Hopf bifurcation and hunting behavior in a rail wheelset with flange contact. Nonlinear Dyn 1998;15(1):15–30.
[12] Yang SP, Shen YJ. Bifurcations and singularities in systems with hysteretic nonlinearity. Beijing: Science Press; 2003.
[13] Kim P, Seok J. Bifurcation analysis on the hunting behavior of a dual-bogie railway vehicle using the method of multiple scales. J Sound Vib 2010;329(19):4017–39.
[14] Lee SY, Cheng YC. Nonlinear analysis on hunting stability for high-speed railway vehicle trucks on curved tracks. ASME J Vib Acoust 2005;127:324–37.
[15] Lee SY, Cheng YC. Influences of the vertical and the roll motions of frames on the hunting stability of trucks moving on curved tracks. J Sound Vib 2006;294(3):441–53.
[16] Cheng YC, Lee SY, Chen HH. Modeling and nonlinear hunting stability analysis of high-speed railway vehicle moving on curved tracks. J Sound Vib 2009;324(1–2):139–60.
[17] Cheng YC. Hunting stability analysis of a full high-speed railway vehicle on curved tracks. Int J Heavy Veh Syst 2012;19(2):151–71.

[18] Zboinski K, Dusza M. Self-exciting vibrations and Hopf's bifurcation in non-linear stability analysis of rail vehicles in a curved track. Eur J Mech A/Solids 2010;29(2):190–203.
[19] Zboinski K, Dusza M. Extended study of railway vehicle lateral stability in a curved track. Veh. Syst. Dyn. 2011;49(5):789–810.
[20] Zboinski K, Dusza M. Bifurcation analysis of 4-axle rail vehicle models in a curved track. Nonlinear Dyn 2017;89(2):863–85.
[21] Hoffmann M. On the dynamics of European two-axle railway freight wagons. Nonlinear Dyn 2008;52:301–11.
[22] Di Gialleonardo E, Bruni S, True H. Analysis of the nonlinear dynamics of a 2-axle freight wagon in curves. Veh Syst Dyn 2014;52(1):125–41.
[23] Zhai W, Wang K. Lateral hunting stability of railway vehicles running on elastic track structures. Trans ASME J Comput Nonlinear Dyn 2010;5(041009):1–9.
[24] Wang KY, Liu PF. Lateral stability analysis of heavy-haul vehicle on curved track based on wheel/rail coupled dynamics. J Transp Technol 2012;2:150–7.
[25] Gao XJ, Li YH, Gao Q. Lateral bifurcation behavior of a four-axle railway passenger car. ASME J Appl Mech 2010;77(6):1–8.
[26] Gao XJ, Li YH, Yue Y. The "resultant bifurcation diagram" method and its application to bifurcation behaviors of a symmetric railway bogie system. Nonlinear Dyn 2012;70(1):363–80.
[27] Gao XJ, Li YH, Yue Y, True H. Symmetric/asymmetric bifurcation behaviours of a bogie system. J Sound Vib 2013;332:936–51.
[28] True H. Multiple attractors and critical parameters and how to find them numerically: the right, the wrong and the gambing way. Veh Syst Dyn 2013;51(3):443–59.
[29] Choi Yeon-Sun, Shin Bum-Sik. Critical speed of high-speed trains considering wheel-rail contact. J Mech Sci Technol 2015;29(11):4593–600.
[30] Nielsen JCO, Igeland A. Vertical dynamic interaction between train and track-influence of wheel and track imperfections. J Sound Vib 1995;187(5):825–39.
[31] Dong RG. Vertical dynamics of railway vehicle-track system [Ph.D. thesis]. Montreal: Department of Mechanical and Industrial Engineering, Concordia University; 1994.
[32] Sun YQ, Dhanasekar M. A dynamic model for the vertical interaction of the rail track and wagon system. Int J Solids Struct 2002;39:1337–59.
[33] Uzzal RUA, Ahmed AKW, Bhat RB. Modelling, validation and analysis of a three--dimensional railway vehicle–track system model with linear and nonlinear track properties in the presence of wheel flats. Veh Syst Dyn 2013;51(11):1695–721.
[34] Meijaard JP, de Pater AD. Railway vehicle systems dynamics and chaotic vibrations. Int J Non Linear Mech 1989;24(1):1–17.
[35] Zeng J, Hu S. Study on frictional impact and derailment for wheel and rail. J Vib Eng 2001;14(1):1–5.
[36] Taheri M, Ahmadian M. Investigation of parameters influencing hunting performance of a railway vehicle with three-piece trucks. In: Proceedings of the 2015 joint rail conference, San Jose, CA, USA, March 23–26; 2015.
[37] Gao XJ, True H, Li Ying-hui. Lateral dynamic features of a railway vehicle. Proc Inst Mech Eng Part F J Rail Rapid Transit 2016;230(3):909–23.
[38] Park Joon-Hyuk, Koh Hyo-In, Kim Nam-Po. Parametric study of lateral stability for a railway vehicle. J Mech Sci Technol 2011;25(7):1657–66.
[39] Tuten JM, Law EH, Cooperrider NK. Lateral stability of freight cars with axles having different wheel profiles and asymmetric loading. J Eng Ind Trans ASME 1979;101(1):1–16.
[40] Zeng XH, Wu H, Lai J, Sheng HZ. Influences of aerodynamic loads on hunting stability of high-speed railway vehicles and parameter studies. Acta Mech Sin 2014;30(6):889–900.
[41] Bozzone M, Pennestri E, Salvini P. Dynamic analysis of a bogie for hunting detection through a simplified wheel–rail contact model. Multibody Syst Dyn 2011;25:429–60.
[42] Cheng YC, Wu Po-Hsien. Optimisation for suspension system of a railway vehicle with a new non-linear creep model developed by uniform design. Int J Heavy Veh Syst 2015;22(2):157–91.
[43] Zhai WM. Vehicle-track coupling dynamics. (third ed). Beijing: Science Press; 2007.
[44] Gao Xue-jun, Li Ying-hui, Gao Q. Hunting motion and bifurcation behavior of six-axle locomotive based on continuation method. J Traffic Transp Eng 2005;5:32–6.
[45] Petersen DE, Hoffmann M. Curving dynamics of railway vehicles, Technical report, Informatics and mathematical modeling. Lyngby: The Technical University of Denmark; 2002.
[46] Kalker JJ. A fast algorithm for the simplified theory of rolling contact. Veh Syst Dyn 1982;11(1):1–13.
[47] Kalker JJ. On the rolling contact of two elastic bodies in the presence of dry friction Doctoral Thesis. Delft, The Netherlands; 1967.
[48] Shen ZY, Hedrick JK, Elkins JA. A comparison of alternative creep force models for rail vehicle dynamic analysis. In: Proceedings of the 8th IAVSD symposium on vehicle system dynamics, dynamics of vehicles on roads and tracks. Swets and Zeitlinger, MIT; 1984. p. 591–605.
[49] Garg VK, Dukkipati RV. Dynamics of railway vehicle systems. New York: Academic Press; 1984.
[50] ArgeCare. Acradschiene: To create or approximate wheel/rail profiles. ArgeCare; 2007. p. 1–97.
[51] Peterka F, Tondl A. Phenomena of subharmonic motions of oscillator with soft impacts. Chaos Solitons Fractals 2004;19(5):1283–90.
[52] Ma Y, Ing J, Banerjee S, Wiercigroch M, Pavlovskaia E. The nature of the normal form map for soft impacting systems. Int J Non Linear Mech 2008;43(6):504–13.
[53] Kundu S, Banerjee S, Ing J, Pavlovskaia E, Wiercigroch M. Singularities in soft-impacting systems. Phys D 2012;241:553–565.
[54] Blazejczyk-Okolewska B, Czolczynski K, Kapitaniak T. Hard versus soft impacts in oscillatory systems modeling. Commun Nonlinear Sci Numer Simul 2010;15:1358–67.
[55] Peterka F, Vacik J. Transition to chaotic motion in mechanical systems with impacts. J Sound Vib 1992;154(1):95–115.
[56] Nordmark AB. Non-periodic motion caused by grazing incidence in an impact oscillator. J Sound Vib 1991;145(2):279–97.
[57] Ivanov AP. Stabilization of an impact oscillator near grazing incidence owing to resonance. J Sound Vib 1993;162(3):562–5.
[58] Hu HY. Detection of grazing orbits and incident bifurcations of a forced continuous, piecewise-linear oscillator. J Sound Vib 1994;187(3):485–93.
[59] Humphries N, Piiroinen PT. A discontinuity-geometry view of the relationship between saddle–node and grazing bifurcations. Phys D 2012;241(22):1911–18.
[60] Kryzhevich S, Wiercigroch M. Topology of vibro-impact systems in the neighborhood of grazing. Phys D 2012;241(22):1919–31.